T.C.
HASAN KALYONCU UNIVERSITY
GRADUATE EDUCATION INSTITUTE
DEPARTMENT OF CIVIL ENGINEERING

EXPERIMENTAL AND NUMERICAL ANALYSIS OF STONE COLUMN TEST ON SILT WITH CONSTUCTION AND DEMOLITION WASTES

Ahmet Haydar CENK

M.Sc. THESIS

GAZİANTEP - 2023

GRADUATE EDUCATION INSTITUTE

THESIS ACCEPTANCE AND APPROVAL FORM

Civil Engineering Department, Civil Engineering Master Programme student Ahmet Haydar CENK prepared and submitted the thesis titled "**Experimental and Numerical Analysis of Stone Column Test on Silt with Constuction and Demolition Wastes**" and defended **successfully** at the date of 20/01/2023 and accepted by the jury as a M.Sc. Thesis.

Position	**Title, Name and Surname**	**University**	**Signature**
Supervisor	Assist. Prof. Dr. Nurullah AKBULUT	Hasan Kalyoncu University	
Jury Member	Prof. Dr. Hanifi ÇANAKÇI	Hasan Kalyoncu University	
Jury Member	Assoc. Prof. Dr. M. Eren GÜLŞAN	University of Gaziantep	

This thesis is accepted by the jury members selected by institute management board and approved by institute management board.

Prof. Dr. M. Serhat YENİCE
Director

TEZ BİLDİRİMİ

Bu tezdeki bütün bilgilerin etik davranış ve akademik kurallar çerçevesinde elde edildiğini ve tez yazım kurallarına uygun olarak hazırlanan bu çalışmada bana ait olmayan her türlü ifade ve bilginin kaynağına eksiksiz atıf yapıldığını bildiririm.

DECLARATION PAGE

I hereby declare that all information in this document has been obtained and presented in accordance with academic rules and ethical conduct. I also declare that, as required by these rules and conduct, I have fully cited and referenced all material and results that are not original to this work.

Ahmet Haydar CENK

23.01.2023

ÖNSÖZ

I would like to thank my academic supervisors Assist. Prof. Dr. Talha SARICI, Assist. Prof. Dr. Nurullah AKBULUT and Assist. Prof. Dr. Gökhan ALTAY for guiding me, helping me complete my master's degree, and great support during the thesis preparation process.…

Ahmet Haydar CENK
Gaziantep-2023

HASAN KALYONCU UNIVERSITY
GRADUATE EDUCATION INSTITUTE
DEPARTMENT OF CIVIL ENGINEERING

EXPERIMENTAL AND NUMERICAL ANALYSIS OF STONE COLUMN TEST ON SILT WITH CONSTUCTION AND DEMOLITION WASTES

AHMET HAYDAR CENK

MASTER THESIS

Supervisor
Assist. Prof. Dr. Nurullah AKBULUT

Co-Supervisor
Assist. Prof. Dr. Talha SARICI

ABSTRACT

The increasing scarcity of adequate engineering properties of land for development, structures, and transportation has led to a growing emphasis on soil improvement. One of the most efficient and effective methods for improving weak soils with low bearing capacity, high compressibility, and high settlement is the use of stone columns. This method is cost-effective, environmentally friendly and improves the soil's stiffness, bearing capacity and making it more resistant to settlement. In this study, construction and demolition waste materials such as natural crushed stone, waste brick, and recycled asphalt pavement were used to construct geosynthetic-encased stone columns with silty soil. Tests were conducted to investigate the bearing capacity and settlement properties of the reinforced soil mixtures. Also, the experimental results were validated using PLAXIS software which is a finite element method. The experimental results showed that using natural crushed stone, waste bricks, and recycled asphalt pavement to reinforce silty soil by stone column method resulted in an increase in bearing capacity of 3.69, 3.57, and 2.64 times, respectively. Overall the results of the other series indicated that the use of waste materials increased the bearing capacity of the soil by up to 6 times, depending on the height of the geogrid and the demolition waste type. Numerical analysis by PLAXIS supported the experimental studies, indicating that construction and demolition waste can be a sustainable and valuable resource for improving soil with geosynthetic-encased stone columns.

Keywords: Soil improvement, stone column, bearing capacity, settlement, experimental, numerical.

HASAN KALYONCU ÜNİVERSİTESİ
LİSANSÜSTÜ EĞİTİM ENSTİTÜSÜ
İNŞAAT MÜHENDİSLİĞİ ANABİLİM DALI

TAŞ KOLON YÖNTEMİ KULLANILARAK SİLT İLE KARISTIRILAN INŞAAT YIKINTI ATIKLARININ DENEYSEL VE SAYISAL ANALİZİ

AHMET HAYDAR CENK

YÜKSEK LİSANS TEZİ

Danışman
Dr. Öğr. Üyesi Nurullah AKBULUT

Eş Danışman
Dr. Öğr. Üyesi Talha SARICI

ÖZET

Arazi kıtlığı, inşaat, yapı ve ulaşım için uygun mühendislik özelliklerine sahip alanların azalmasına neden olmuştur. Bu durum zemin iyileştirmesine olan önemi artırmıştır. Zayıf zeminlerin düşük taşıma kapasitesi, yüksek sıkışabilirlik ve oturma özellikleri, taş kolon kullanımını etkili ve verimli bir yöntem haline getirmektedir. Bu yöntem, uygun maliyetli, çevre dostu ve zemini daha dayanıklı hale getirerek rijitlik ve taşıma kapasitesini artırmaktadır. Bu çalışma, inşaat yıkım atıkları ve geosentetik ile güçlendirilmiş siltli zemin karışımlarının oturma özellikleri ve taşıma kapasiteleri incelemek amacıyla farklı kobinasyonda deney serilerini içermektedir. Ayrıca, çalışma kapsamında deneysel sonuçlar PLAXIS yazılımı kullanılarak, sonlu elemanlar yöntemiyle de sayısal olarak doğrulanmıştır. Siltli zeminin taş kolon yöntemiyle güçlendirilmesinde kullanılan kırmataş, atık tuğla ve geri dönüştürülmüş asfalt ile yapılan deneysel çalışmada, taşıma kapasitesinde sırasıyla 3.69, 3.57 ve 2.64 kat artış olduğu gözlemlenmiştir. Diğer deney serilerinin sonuçları incelendiğinde, kullanılan geosentetik malzemenin yüksekliği ve inşaat yıkım atığı türüne bağlı olarak taşıma kapasitesinin 6 kata kadar arttığı görülmüştür. PLAXIS yazılımı ile gerçekleştirilen sayısal analizler, deneysel çalışmaları doğrulamış ve geosentetik malzemelerle güçlendirilen inşaat ve yıkım atıklarının taş kolon yöntemiyle zemin iyileştirmesi için değerli ve sürdürülebilir bir kaynak malzemesi olabileceğini göstermiştir.

Anahtar Kelimeler: Zemin iyileştirme, taş kolon, taşıma kapasitesi, oturma, deneysel, sayısal

TABLE OF CONTENTS

LIST OF TABLES

LIST OF FIGURES

ABBREVIATIONS OR SYMBOLS LIST

UR	Unreinforced (silty soil)
NA	Natural Aggregate (crushed stone)
RAP	Recycled Asphalt Pavement
WB	Waste Brick
G-NA-SC	Stone column sample encased with 25 cm height geogrid and reinforced with natural crushed stone
G/2- NA-SC	Stone column sample encased with 12.5 cm height geogrid and reinforced with natural crushed stone
G-WB-SC	Stone column sample encased with 25 cm height geogrid and reinforced with waste bricks
G/2-WB-SC	Stone column sample encased with 12.5 cm height geogrid and reinforced with waste bricks
G-RAP-SC	Stone column sample encased with 25 cm height geogrid and reinforced with recycled asphalt pavement
G/2-RAP-SC	Stone column sample encased with 12.5 cm height geogrid and reinforced with recycled asphalt pavement
VESC	Vertically Encased Stone Column
HRSC	Horizontally Reinforced Stone Column
GESC	Geosynthetic Encased Stone Column
$\mathbf{C_u}$	Undrained shear strength
MPa	Megapascal
kPa	Kilopascal
kg	Kilogram
cm	Centimeter
mm	Millimeter
m	Meter
MH	High plasticity silt
Gs	Specific gravity
ϕ	Internal angle of friction
c	Cohesion
γ_{max}	Maximum dry unit weight

γ_{min}	Minimum dry unit weight
ID	In the manufacturing direction (for Geogrids)
IDD	Perpendicular to the manufacturing direction (for Geogrids
CBR	California Bearing Ratio
AASHTO	American Association of State Highway Transportation Officials
ASTM	American Society for Testing and Materials
D	Tank diameter
d_f	Foundation diameter
γ_s	Solid particles unit weight
γ_n	Natural unit weight
γ_{sat}	Saturated unit weight
γ_{unsat}	Unsaturated unit weight
E	Young's Modulus
W_{wet}	Wet weight
ν	Poisson's ratio
ψ	Dilation angle

1. INTRODUCTION

1.1. General

Geotechnical engineering studies the soil problems and applies the soil improvement methods to improve the engineering properties of of weak soils. This is done to prevent buildings from differential settlement and to increase stability against failure problems. In the last years the studies have focused on reducing construction waste and utilizing these wastes in soil reinforcement methods. Recycled materials have been incorporated into techniques that use natural resources, with the goal of promoting sustainability in geotechnical engineering and minimizing the use of natural resources. Construction and demolition waste materials such as concrete, asphalt, and brick have been widely used in geotechnical engineering methods. Also, geosynthetic materials have become a popular choice in the construction of stone columns. Geosynthetic materials such as geogrids, geotextiles, geomembranes, geocomposites are used in various applications, ranging from coastal and harbor armoring to soil reinforcement methods. It has been observed that the use of geosynthetic materials increases the bearing capacity of the stone column method (Malarvizhi & Ilamparuthi, 2007; Safiuddin et al. 2010).

The primary soil improvement methods used to enhance soil conditions are dynamic compaction, stone columns, pre-loading with vertical drains, grouting, deep mixing, geotextile, reinforcement with piles, electro-osmosis and thermal methods. The method of using stone columns is a way to reinforce soil and increase its bearing capacity. It is a solution for soils that are experiencing settlement issues. This method has gained popularity worldwide and is now considered one of the most famous soil reinforcement methods.

The construction method for stone columns can be categorized into two methods: replacement and impact. The replacement method involves compacting non-cohesive soils with less than 10% fine grain. This method can be done either dry or wet, with the wet method being the preferred and cost-effective technique for soft to hard consistency soil and high ground water. The dry method is more suitable for fields with hard soil and low water level. The impact method involves using soil vibrators to compact soil into a column shape. This method is effective for non-cohesive soils and is influenced by the ground water level.

Urbanization, population growth, and technological advancements that improve living standards have led to a rise in the amount of construction and demolition waste. The use of construction and demolition waste has various environmental benefits, including reducing greenhouse gas emissions, saving water, conserving energy and natural resources, and preventing pollution. While previous research has focused on using recycled asphalt shingles, crushed concrete aggregates, and crushed bricks for geotechnical applications, little has been reported on their performance when mixed with a silty soil and encased with geogrid. Recycling and reusing construction and demolition waste as a soil improvement technique is an alternative that allows for the utilization of multiple waste materials at once. This aligns with the principle of high-quality waste management, which aims to safely reuse waste materials. Therefore, studies have been conducted to identify the potential use of these materials for road stabilization (Arulrajah et al., 2012; Modarres and Nosoudy, 2015).

The thesis aims to achieve two main objectives. Firstly, it intends to estimate the bearing capacity of a silty soil that is mixed with construction demolition wastes and encased by geogrid using the stone column method. Secondly, it aims to compare and validate the experimental results obtained by PLAXIS for unreinforced silty soil with those of reinforced with construction and demolition wastes.

1.2. Objective of the Study

The main objectives of the thesis are;

- to investigate the bearing capacity and settlement behavior of shallow foundations on a silty soil, both with and without reinforcement using stone column method.
- to make an experintal study of producing stone column samples with and without geogrid encasement using crushed natural stones, recycled asphalt pavement, and waste brick materials.
- to make a numerical analysis using PLAXIS software for validating and comparing the experimental results.

1.3. Organization of the Study

Chapter 1: This chapter covered topics related to soil improvement techniques and stone column method. It also explored the utilization of construction demolition and waste materials in the stone column method, as well as the role of geosynthetic materials in enhancing its strength.

Chapter 2: As a result of the literature review, the studies about soil improvement of stone column method are given in this chapter.

Chapter 3: This chapter involved conducting both experimental studies and numerical analyses. It also provides a description of the properties of the materials used in the experimental studies and the experimental setup. Additionally, it explains the usage of the PLAXIS software in the numerical analysis.

Chapter 4: In this study, the results obtained from the experimental study and numerical analysis are interpreted and evaluated. The results are presented in the form of figures and graphs.

Chapter 5: This chapter presents the outcomes of both numerical analysis and experimental studies conducted on the bearing capacity and settlement behavior of stone column method.

2. LITERATURE REVIEW

2.1. General

As a result of the literature review, studies conducted with the stone column method was provided chronologically in this section.

Zahmatkesh and Choobbasti (2010) analyzed the behavior of reinforced clay soil with the stone columns in their study. It was hypothesized that clay layer was homogeneous. Mohr-Coulomb model was applied. The distance between stone columns used and the strain rate were examined. The increase in the strain rate was proved to have a low impact on the Settlement Reduction Ratio.

Kurt (2011) compared the results with PLAXIS 2D Finite Element Method by conducting a load test for the difference between impact crushed stone column and stone column in his thesis. The rigidness of stone columns formed with the displacement method was determined to have four times higher value compared to the ones formed with pre-drill. He concluded that the impact crushed stone column provides between 2.2 and 8.8 times better peformance than normal stone columns.

In their study, Yaswant et al. (2011) applied stone column method by using sea clay as a soil. The behavior under the cyclic and static load was examined. The diameter of stone columns was determined 100 mm and the grain size was preferred between 2 mm and 8 mm. As a result of this experiment, the increase in strength was observed under the impact of cyclic and static load on the soil used stone columns.

Jin Man Kim et al. (2012) discovered that application of seismic load to the soil reinforced with stone columns will demonstrate less deformation compared to the unreinforced soil in their experimental study.

Marto et al. (2013) carried out numerical analysis of geogrid-encased stone column and uncased column in their experiments. They used Plaxis Package Software. It was observed that the stone column takes on more load regarding small size stone columns, the strength of stone column constructed with geogrid increases and lateral bulging decreases.

Adeli (2013) acquired the requested data by analyzing stone columns and applying numerical and analytic methods. Through changing properties such as the diameter and

distance of stone columns, modulus of elasticity, the properties effect on the reinforcement of soil were investigated. Applying the results obtained, he concluded the most appropriate stone column's diameter and replacement. He patterned his study with the finite element method.

Das et al. (2013) manufactured stone column with the usage of clayey-silty sand soil in their study. The physical properties of clayey-silty was determined, and geosynthetics material was used during the construction of stone column. According to obtained data, the bearing capacity was observed to increase when the diameter of column was increased in the construction of geosynthetic stone column. The load replacement behavior of the loaded area was linear. In the case of layered soil, the bearing capacity was viewed to decrease as the column diameter increases.

Sarıcı et al. (2013) conducted 12 experiments about the reinforced and unreinforced clay soil in their study. The obtained results demonstrated that as the value of undrained shear strenght (cu) increased, the bearing capacity increased as well. Coating stone column with geosynthetic improved its performance and decreased the settlement. When the rigidness of geosynthetic used for coating the stone column increased, its contribution to the bearing capacity was found to increase due to limiting lateral bulging of stone column under load.

Demir et al. (2013) preferred stone column method for the reinforcement of clay soil. According to the results they obtained, the stone column improved the bearing capacity of clay foundation. The stone column with the large diameter has higher bearing capacity than the one with small diameter

Afshar & Ghazavi (2014) used reinforced and unreinforced stone columns which were 60mm, 80mm, and 100mm diameters. They studied the bearing capacity for the vertical encased stone columns (VESC) and horizontal reinforced stone column (HRSC). Consequently, when both circumstances were analyzed, it was observed that the bearing capacity of stone columns increases and lateral bulging decreases.

Demir & Sarıcı (2016) examined the effect of stone column's performance in the soft soil foundation by using geogrid coating in their studies. Numerical and experimental studies were conducted. The Plaxis finite element method was preferred as numerical studies were conducted. The stone column with geogrid coating was improved the bearing

capacity of the soil. Lateral bulging was generally observed to be more on the top of stone column.

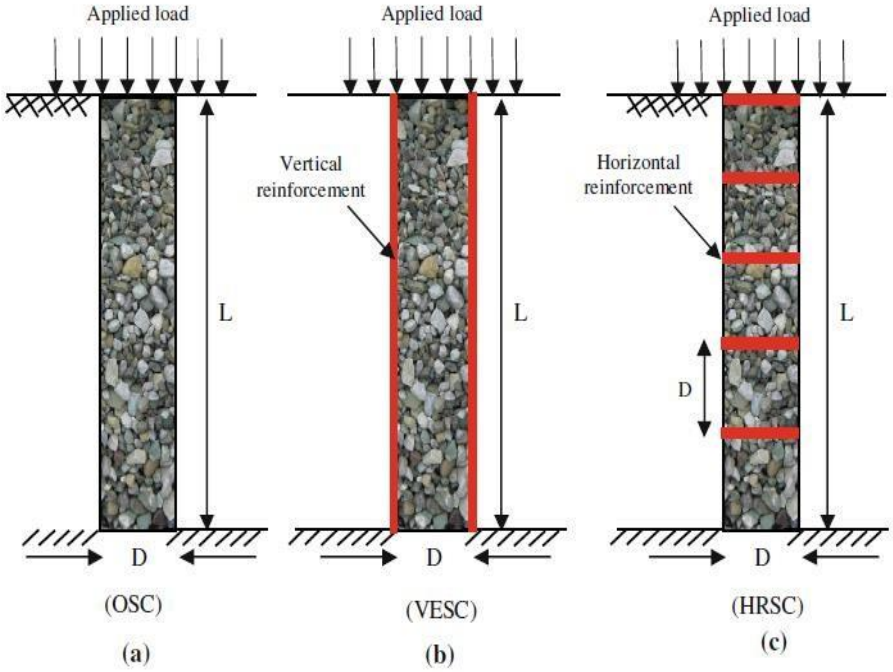

Figure 2. 1. Photo of a) ordinary granular column, b) vertically encased granular column and c) horizontally reinforced granular column (Afshar and Ghazavi 2014)

Demir & Sarıcı (2017) examined the bearing capacity of geogrid-encased stone column in their study. The Plaxis finite element method software was used. In their study, the properties were analyzed such as the impact of stone column's diameter preferred, the angle of friction of stone and the length of geogrid encased. It was analyzed through Mohr-Coulomb method. It was stated that the bearing capacity increased with the stone column used on the clay soil, the geogrid encased stone column increased the bearing capacity of the soil, and the lateral bulging of the geogrid encased stone column decreased.

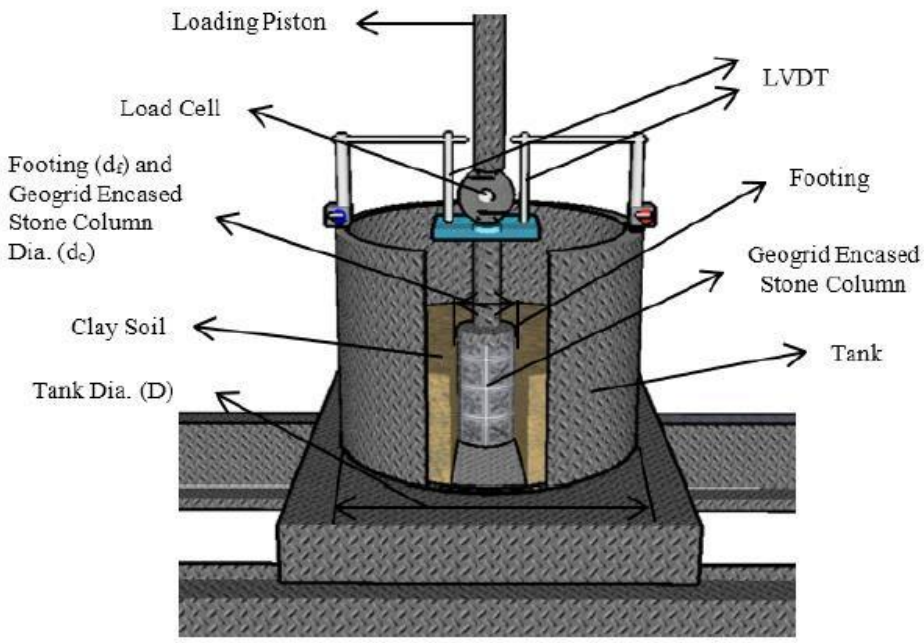

Figure 2.2. Model view of plate loading set-up (Demir and Sarıcı, 2017)

Rajesh (2017) conducted research to examine the deformation effect of the height of stone column and the length of geosynthetic coating used to cover stone columns. Plaxis Finite Element Method was used. As a conclusion, a significant decrease in the lateral bulging was observed in the study.

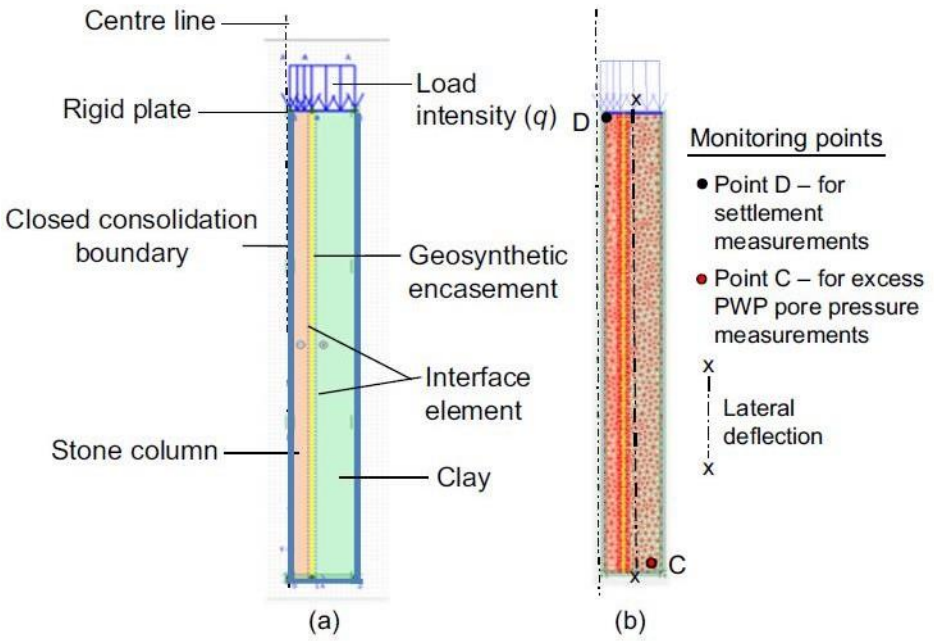

Figure 2.3. PLAXIS view of a) axisymmetric unit cell, b) mesh model (Rajesh, 2017)

Reddy & Mohanty (2017) examined the condition of the soil under the seismic load by both using and not using stone column method in their study. The survey studied replacement, acceleration, and the change in the different locations of shear stress. Considering the test results, the soil reinforced with the stone column decreased the deformation and pore pressure compared to unreinforced soil. In the studies, the 3D Finite Element Software OpenSeesPL was preferred.

Fahmi & Kolosov (2018) explored the circumstances of soil reinforcement between the geogrid encased stone column and stone column method in their study. According to the study, the models subjected to cyclic upload tested under 5mm/sec loading rate reached the failure level slowly compared to the ones tested under 10mm/sec. The experiments were analyzed with the finite element method in the computer environment.

Yoo & Abbas (2020) conducted research about the construction of geosynthetic encased stone column in their study. The hardness of geosynthetic materials and the properties of cyclic loading were emphasized. It was observed that the load transfer of the stone column operating under static upload had more than the condition of cyclic load and the rate of concentration increased %25.

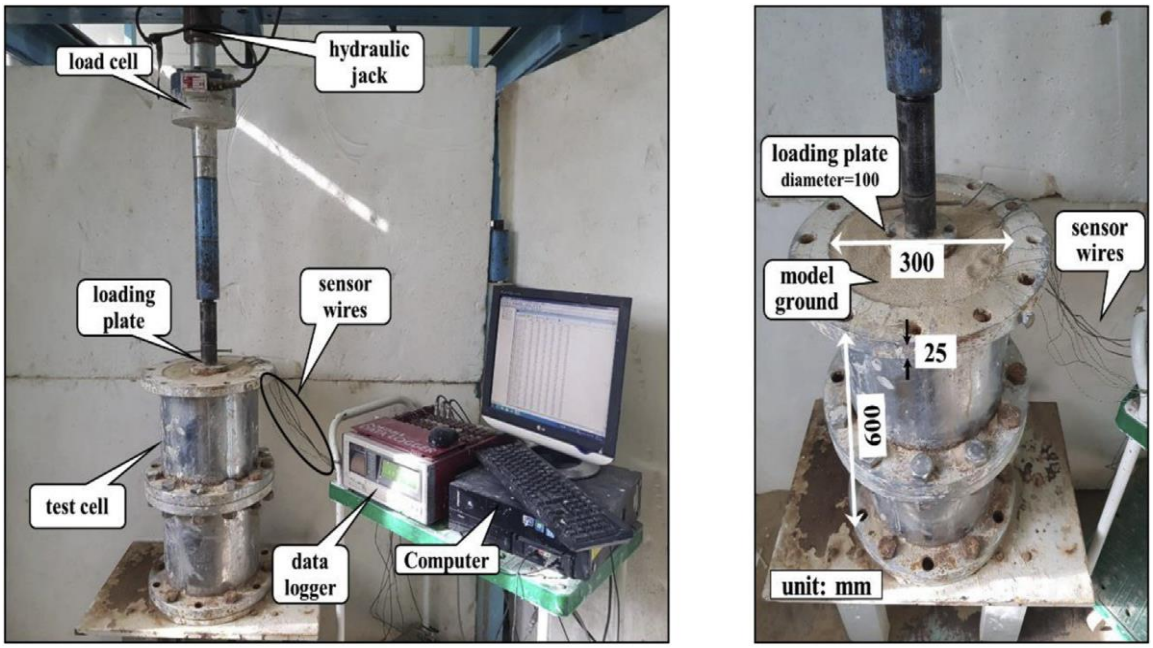

Figure 2.4. Photo of a) data acquisition system and b) geosynthetic encased stone column sample (Yoo and Abbas, 2020)

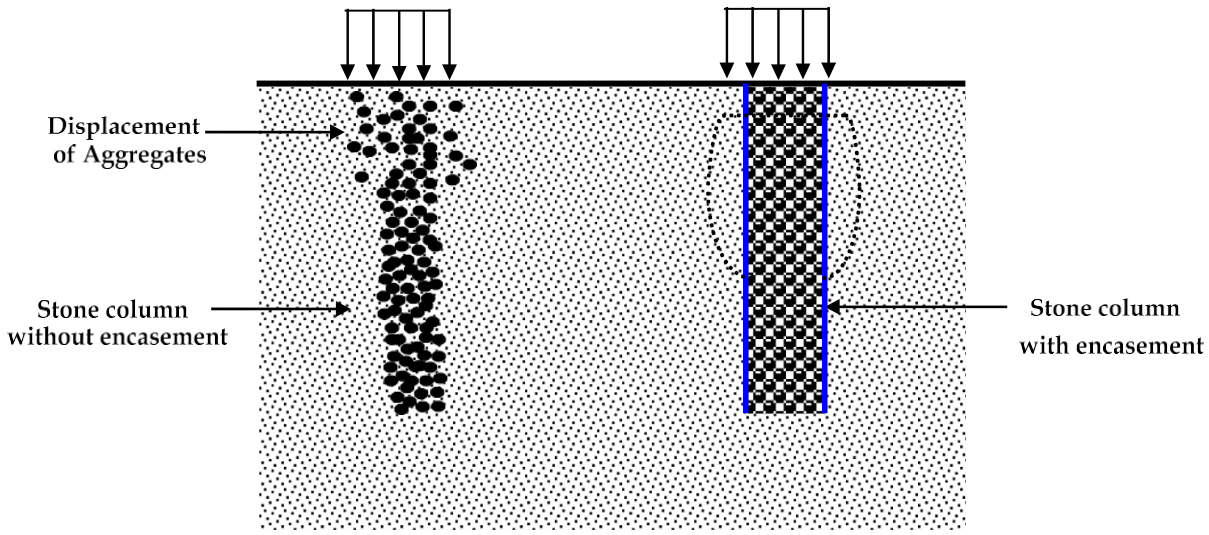

Figure 2.5. Schematic view showing the mode of failure of stone column with and without encasement (Rathod et al., 2021).

Rathod et al. (2021) conducted experiments to increase the bearing capacity of soil in their study. They examined that the bearing capacity of the soil reinforced with stone column method increased two times. The lateral bulging of the polypropylene encased stone columns decreased by half. The handling costs of polypropylene coating material was three times affordable considering other geotextile coating materials.

3. MATERIALS AND METHOD

3.1. Materials used during the Study

This thesis study involved the use of both experimental and numerical analysis methods. In this section, the characteristics of the experimental setup and materials utilized during the experiments were outlined, along with details regarding the application of PLAXIS software in the numerical analysis.

3.1.1. Silty soil

The silty soil used in the experimental studies for stone columns was obtained from an area in Kiltepe neighborhood of Yeşilyurt, Malatya in Turkey where there was no construction. A crawler excavator was used to open an inspection pit in the field where the silty soil was located, and the samples were then transported to the Civil Engineering Department of Inonu University. The silty soil was extracted from a depth of 2.0 - 2.5 meters. Figure 3.1. demonstrates the sampling site.

Figure 3.1. Photo of the silty soil used during the study

The unconfined compression test was conducted based on the ASTM-D2166 guide to determine the undrained shear strength (c_u) of silt soil with %26, %29 and %32 water content. Before the experiment, the silt soil was prepared in the containers

according to the desired water content ratio. The experiments were started respectively %26, %29 and %32 water content and results were listed. At the end of the experiments, each sample's water content was checked. Figure 3.2. shows the preparation of sample for the unconfined compression test. The water content based on undrained shear strength was shown on the Table 3.1.

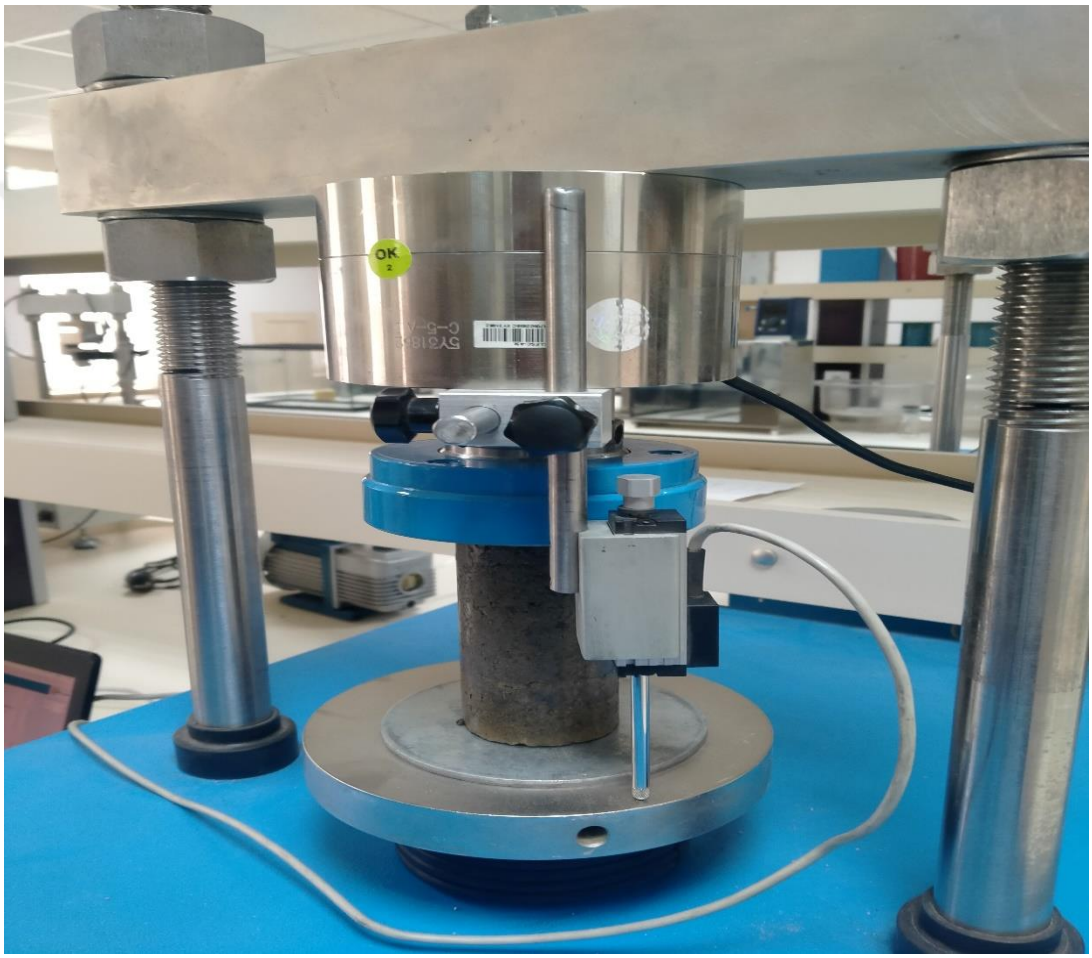

Figure 3.2. Photo of the unconfined compression equipment

The Pycnometer test for silt soil was performed according to ASTM-D854 shown in Figure 3.3. and Figure 3.4. The specific gravity value was determined with the Pycnometer test. The silt material weighed to the desired extent and water were added to calibrated Pycnometer. Vacuum pumping was performed from the neck of Pycnometer to evacuate the air from the soil reducing the presence of air voids. An easy evacuation of air was provided through shaking the Pycnometer slowly. The weighing based on the

related standard was completed. Consequently, the specific gravity was determined through the formula based on the related standards. It is demonstrated in the table 3.1.

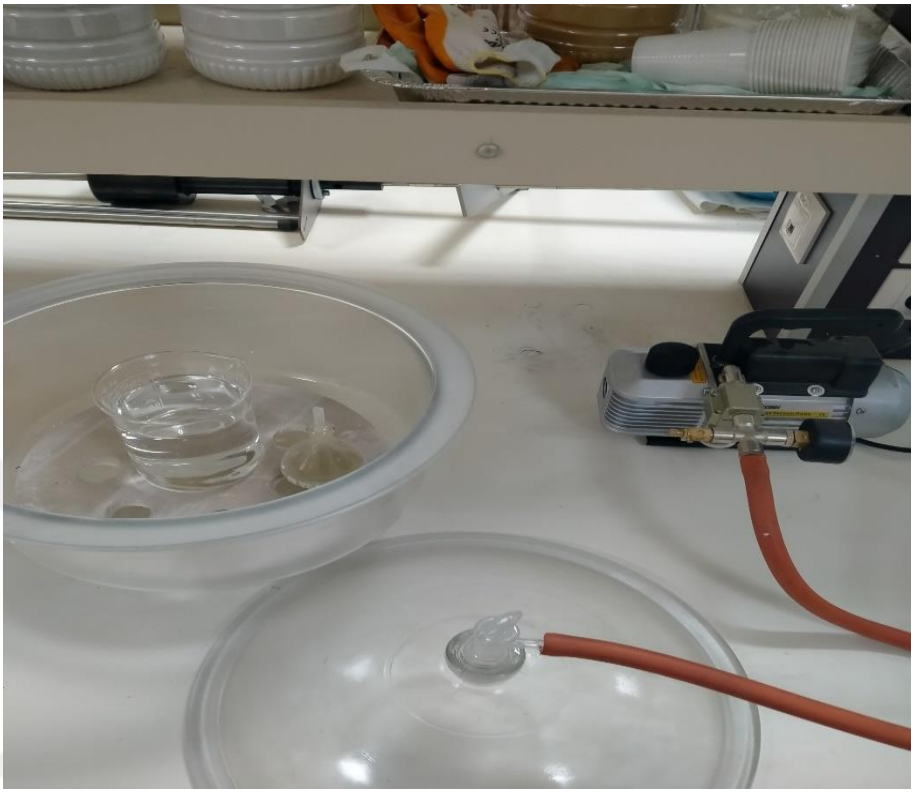

Figure 3.3. Photo of the elements used during the pycnometer test

Figure 3.4. Photo of the weighing measurement during the pycnometer test

Atterberg limits was examined based on ASTM-D2487 standards. Figure 3.5 is showing the liquid limit and plastic limit tests conducted during the experimental study.

(a)

(b)

Figure 3.5. Photo of the Atterberg limit tests a) liquid limit and b) plastic limit

The gradation curve is presented in Figure 3.6, depicting the results of sieve analysis and hydrometer tests conducted according to ASTM-D422 and ASTM-D1140 on the silt soil. Besides, according to these test results, the soil class MH (high plasticity silt) was determined.

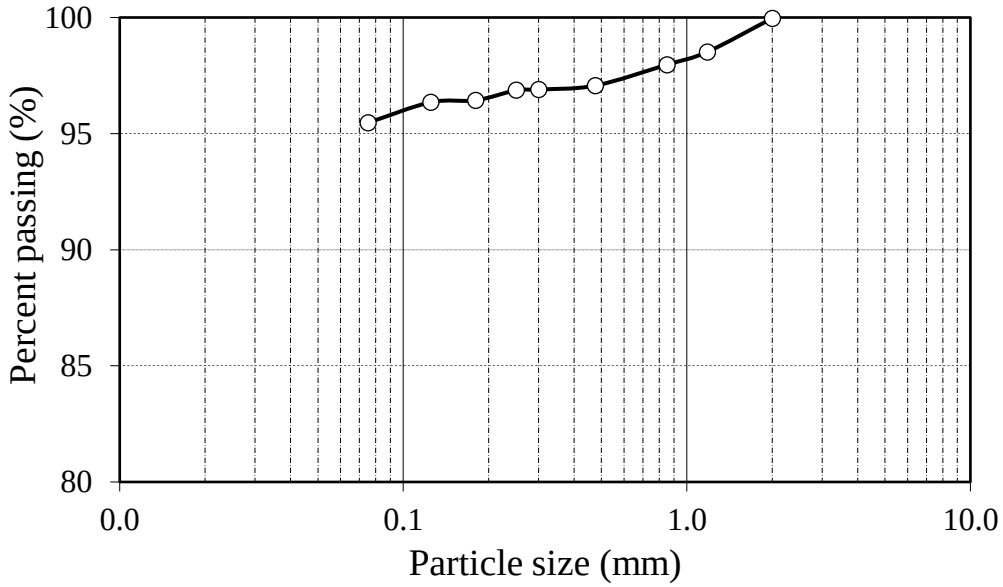

Figure 3.6. Sieve analysis of the silty soil

Table 3.1. Engineering properties of the silty soil

Parameter	Value		
Specific gravity (G_s)	2.64		
Liquid limit (%)	55		
Plastic limit (%)	32		
Classification	MH		
Water content (%)	26	29	32
Undr. shear strength	93	75	55

3.1.2. Natural crushed stone

The natural crushed stone was used in the stone column method. The grain size of natural crushed stone was implemented according to the detailed literature review (Deb. et al, 2010). The gradation curve was generated by performing sieve analysis on the natural crushed stone in accordance with ASTM-D422. The grain diameter of natural crushed stone was examined to be between 2 mm to 6 mm. The gradation curve obtained from the sieve analysis was displayed in the Figure 3.7. The Pycnometer test was conducted on the natural crushed stone in accordance with ASTM-D854 standards. The minimum and maximum densities were determined to identify the loose and dense conditions of the natural crushed stone.

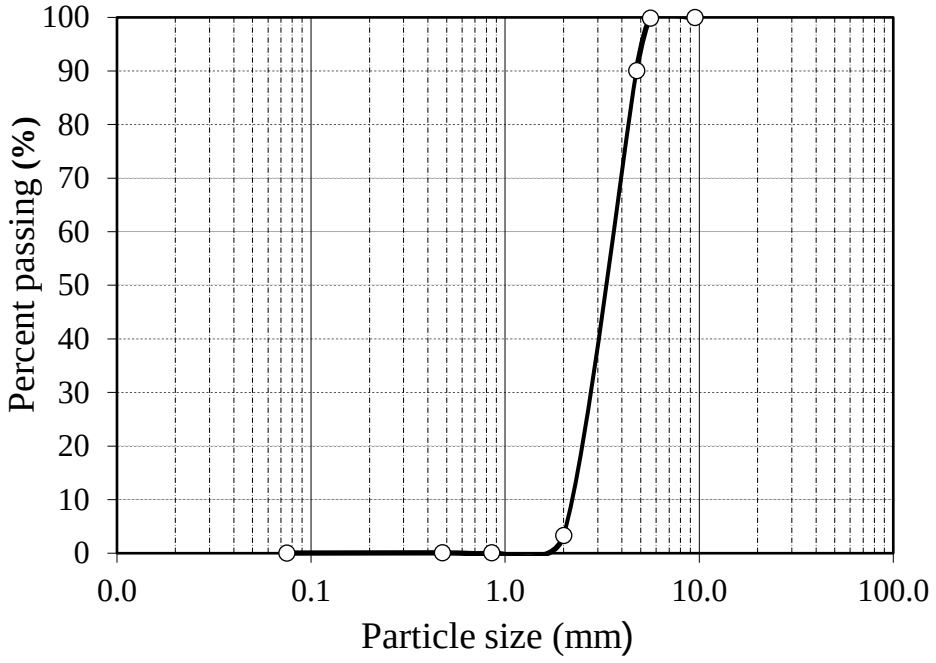

Figure 3.7. Sieve analysis of the natural crushed stone

The tests conducted to determine the properties of natural crushed stone was decided and commented on in accordance with the standards, shown in the Table 3.2.

Table 3.2. Engineering properties of the natural crushed stone

Parameter	Value
Specific gravity, (G_s)	2.73
Bulk density (γ) (kN/m^3)	16.15
Max. dry unit weight, (γ_{max}) (kN/m^3)	16.28
Min. dry unit weight, (γ_{min}) (kN/m^3)	14.95
Cohesion, (c_u) (kPa)	1.56
Internal angle of friction, (ϕ) (^{o})	47.81

3.1.3. Waste brick

The construction waste has caused environmental pollution in conjunction with the urbanization in developing countries. One of the biggest environmental issues of the world was the storage and disposal of construction and demolition waste. Many countries struggle to find a permanent solution for this situation. Therefore, it was considered that these wastes could be recycled or used as material in the soil reinforcement methods. Thereby, it will contribute considerably to the economy of countries by both eliminating waste production and removing the need for material production. Within the context of this thesis, the waste stone column, a type of the demolition waste, was used. The waste brick grain size was preferred between 2 mm to 6 mm as in the case of natural crushed stone. The gradation curve was generated by performing sieve analysis on the waste brick in accordance with ASTM-D422 and illustrated in Figure 3.8. The Pycnometer test was conducted on waste brick according to ASTM-D854 standard. The minimum and maximum densities were determined to identify the loose and dense conditions of the waste brick.

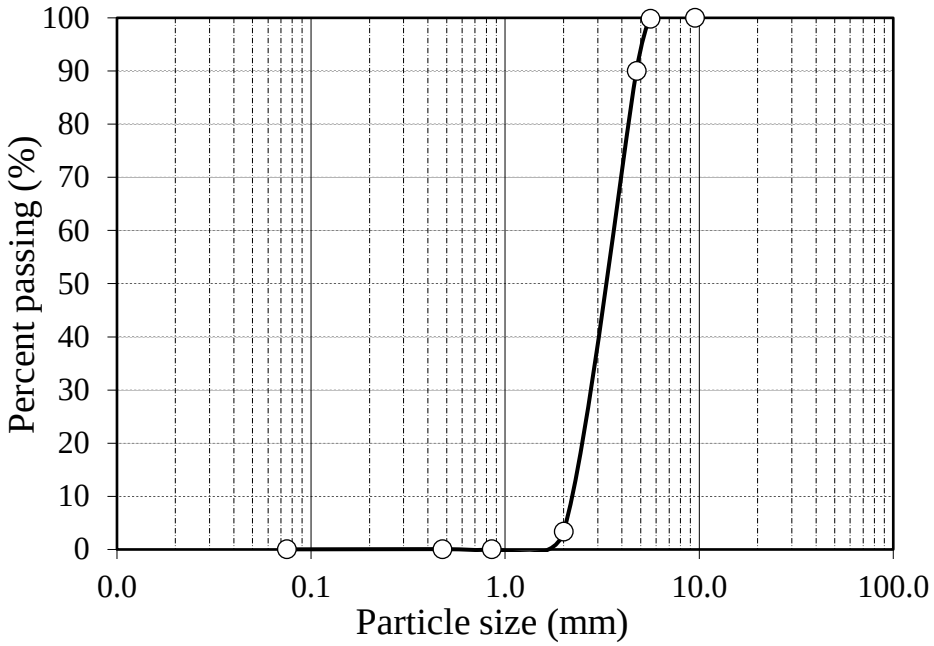

Figure 3.8. Sieve analysis of waste brick

The tests conducted to determine the properties of waste brick was decided and commented on in accordance with the standards, shown in the Table 3.3.

Table 3.3. Engineering properties of the waste brick

Parameter	**Value**
Specific gravity, (G_s)	2.61
Bulk density (γ) (kN/m^3)	12.12
Max. dry unit weight, (γ_{max}) (kN/m^3)	12.33
Min. dry unit weight, (γ_{min}) (kN/m^3)	10.01
Cohesion, (c_u) (kPa)	14.68
Internal angle of friction, (ϕ) (^{o})	41.03

3.1.4. Recycled asphalt pavement

Transportation and infrastructure are one of the most important units of the construction sector. Transportation is a significant communication tool connecting cities and countries. The common units of it are constructions such as roads, bridges, viaduct, and highways. The material commonly used in these foundational constructions was recycled asphalt pavement. The recycled asphalt pavementmaterial was being laid on the routes that form these foundational structures. The asphalt was produced to a standard quality in the building site and used in the structures. In the case of roads, bridges,

viaducts, highways, and similar structures, the asphalt material becomes dysfunctional after reaching the end of their service life. In this circumstance, they become waste.

Within the scope of this thesis, recycled asphalt pavement, which was one of the constructional wastes, has been utilized. The grain size of recycled asphalt pavement was preferred between 2 mm to 6 mm as in the case of natural crushed stone. The gradation curve was generated by performing sieve analysis on the recycled asphalt pavementin accordance with ASTM-D422, and it was illustrated in Figure 3.9. The Pycnometer test was conducted on Recycled asphalt pavement based on the ASTM-D854 standard. The maximum and minimum densities were determined to identify the loose and dense conditions of recycled asphalt pavement.

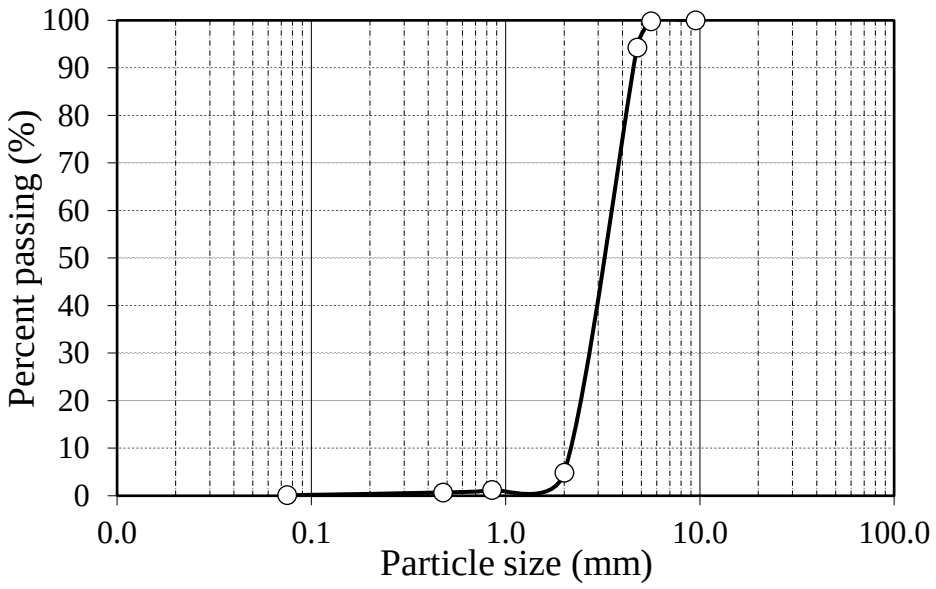

Figure 3.9. Sieve analysis of recycled asphalt pavement

Table 3.4. Engineering properties of the recycled asphalt pavement

Parameter	**Value**
Specific gravity, (G_s)	2.65
Bulk density (γ) (kN/m^3)	15.11
Max. dry unit weight, (γ_{max}) (kN/m^3)	15.22
Min. dry unit weight, (γ_{min}) (kN/m^3)	13.29
Cohesion, (c_u) (kPa)	9.92
Internal angle of friction, (ϕ) (^{o})	39.48

3.1.5. Geogrid

In the experimental studies, geogrid was used for the encasement of the stone column (to cover the stone column' lateral surface). Considering the studies conducted on literature, the performance of the stone column was increased (Demir & Sarıcı, 2017; Sarıcı et al., 2017; Demir & Sarıcı, 2016; Gniel & Bouazza, 2009; Gniel & Bouazza, 2010; Fattah & Majeed, 2012; Gu et al., 2016; Gu et al., 2017; Gu et al., 2020; Gu et al., 2022; Debnath & Dey, 2017; Debnath & Dey, 2018; Xu et al., 2021; Tan et al., 2021; Ghanizadeh et al., 2023; Pandey et al., 2020; Jianfeng et al., 2019; Paul & Ponomarjow, 2004; Kwa et al., 2018; Elsawy et al., 2010).

The geogrid was supplied from YMN Group Company. The geogrid used in the experiment was illustrated in Figure 3.10. The properties of geogrid were supplied and presented detailed in Table 3.8. In the detailed examination, the company has presented the type of material, unit surface weight, tensile strength, tensile strength at 2% elongation (ID/IDD), and clearance dimension (mm x mm) in table format.

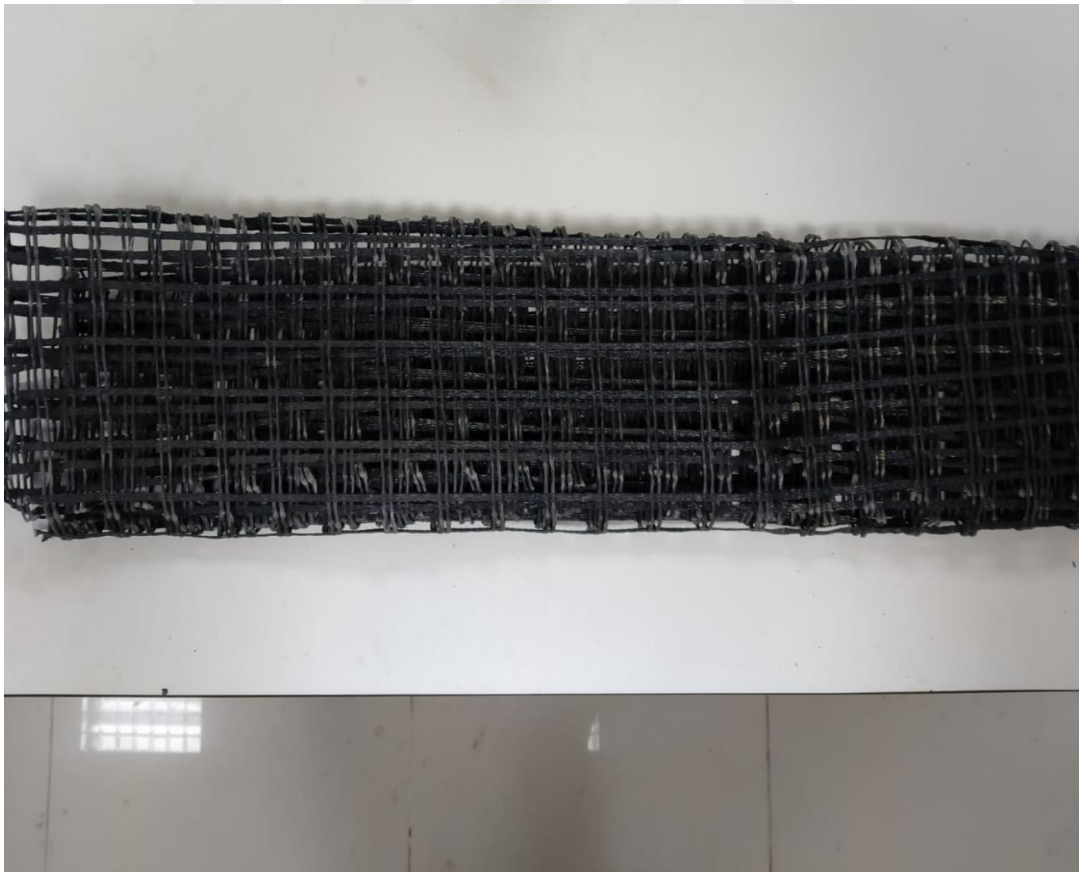

Figure 3.10. Photo of the geogrid used during the experimental study

Table 3.5. Engineering properties of the geogrid

Properties	Value
Material type	Polyester
Unit weight of Surface (g/m^2)	230
Tensile strength	≥30
Nominal elongation ID/IDD (%)	12(±2)
Clearance dimension (mm x mm)	25x25
Internal angle of friction, (ϕ) (^{o})	39.48

3.2. Engineering Properties of the Construction and Demolition Wastes

3.2.1. Shear strength test

The shear box test was conducted on natural crushed stone (NA), waste brick (WB) and recycled asphalt pavement (RAP), and the experimental setup was illustrated in Figure 3.11. The shear box test was carried out using a large-scale device manufactured by DOTEK Company. At the end of the shear box test, the angle of friction and cohesion of the materials was found. The obtained data was utilized in the PLAXIS software as an input. The shear box test results were shown in Figure 3.12.

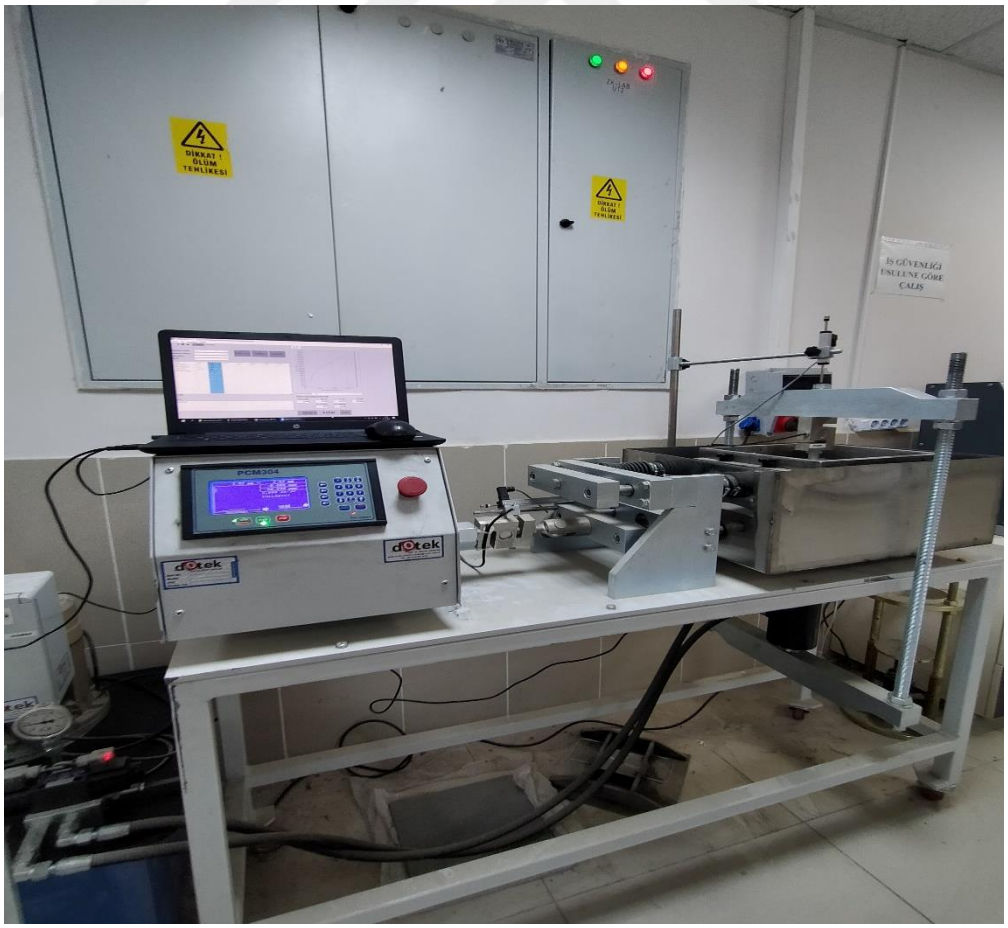

Figure 3.11. Photo of the direct shear testing equipment

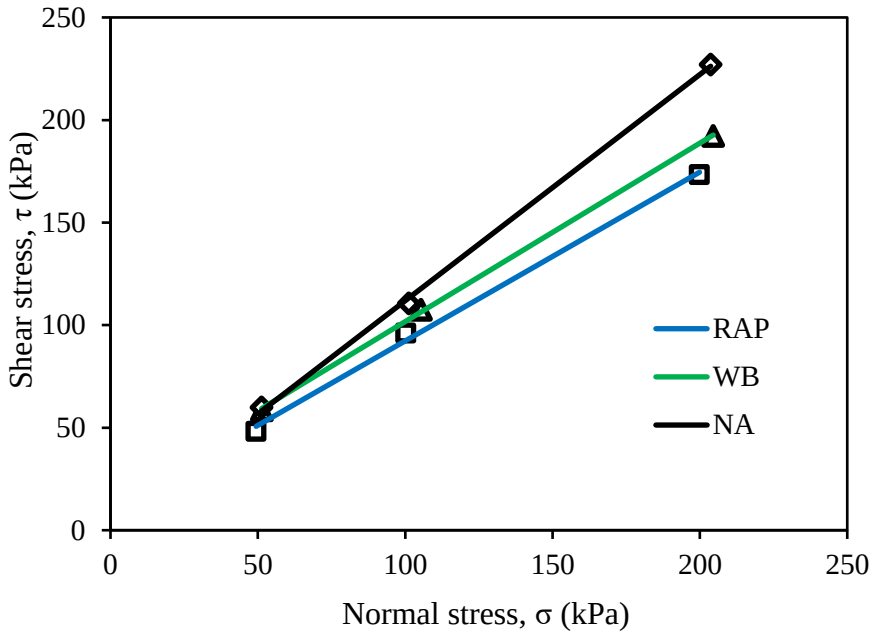

Figure 3.12. Direct shear test results for the materials used during the study

The impact test was conducted on the natural crushed stone, waste brick, recycled asphalt pavement, and the findings were illustrated in Table 3.9. The experimental set-up was presented in Figure 3.13.

Table 3.6. Impact strength properties of the materials

Construction and Demolition Wastes	Impact strength (%)
Natural crushed stone	26.09
Recycled Asphalt Pavement	34.52
Waste Brick	46.48

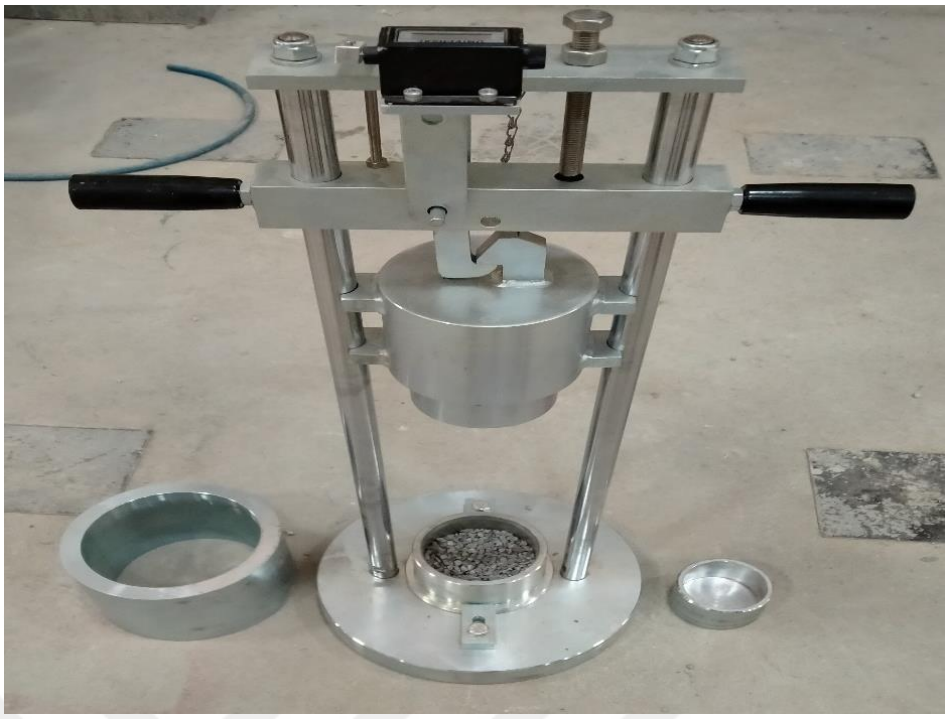

Figure 3.13. Photo of impact strength testing equipment

3.3. Components of the Experimental Set-up

3.3.1. Steel frame system

The plate loading test was implemented using the steel frame system. The tests were conducted in a rigid environment. The load frame was fabricated from I-profiles and has a maximum load capacity of 20 tons. It has been manufactured by DOTEK company. The structural component of the system consists of data logger, load cell, steel tank, displacement sensor, load system control panel, and computer. Figure 3.14. illustrates the steel frame system and the structural components of it.

Figure 3.14. Photo of the steel frame used during the study

3.3.2. Data logger

During the test, the loads measured by displacement sensors and load cells, as well as the vertical displacements, were transferred to the computer software system via the ELE brand data logger device. The transformed data was converted into numerical values. The converted data was listed in the table form. The data logger used in tests was presented in Figure 3.15.

Figure 3.15. Photo of the data logger used during the tests

3.3.3. Displacement gauges (LVDTs)

The displacement gauges were used to prevent vertical displacement in the model foundation as the plate loading test was implemented. The displacement sensor was firmed to the test tank through magnets. The average of the values taken from these two displacement sensors were considered to measure the displacement of model foundation. The calibration of displacement sensors was performed in the computer environment to correctly measure. The displacement sensors used in tests, shown in Figure 3.16. (Sarıcı, 2014).

Figure 3.16. Photo of the displacement gauges

3.3.4. Load cell

The load cell with a load capacity of 1500 kg was preferred as conducting the plate loading test on the silt soil. The data of load cell was transformed into data loggers. The load cell was used for both tensile and pressure measurement in the plate load test. Prior to conducting the tests, the calibration was performed in the computer environment. Figure 3.17 illustrated the load cell in detail.

Figure 3.17. Photo of the S-type load cell

3.3.5. Circular steel tanks

During the plate loading test, three circular steel tanks with a diameter of 30 cm named as A, B, and C were preferred. Figure 3.18 presents the tanks used in the test.

Figure 3.18. Photo of the circular steel tank

3.3.6. Foundation model

The foundation with a diameter of 5 cm was used in the plate loading tests. Figure 3.19. illustrates the model foundation with a diameter of 5 cm used in tests.

Figure 3.19. Photo of the foundation model

3.3.7. Loading system

The load system can move in both upward to downward direction with the desired speed thanks to the load system. The speed was happened to be 1 mm/sec speed in the plate loading tests. Figure 3.20. presents the load system in detail.

Figure 3.20. Photo of the loading system

3.3.8. Stone column mold

For the plate loading test, a steel stone mold with a diameter of 5 cm and a length of 30 cm was used to apply the stone column method inside the silt soil. The impact method was performed to apply the stone column method. To conduct this method, steel tamper with the same diameter of the stone column was preferred. Figure 3.21. shows the stone column mold and tamper in detail.

(a) **(b)**

Figure 3.21. Photo of a) the stone column mould and b) the tamper

3.4. Implementation and Preparation of the Samples

The experiments were implemented in the Geotechnic Laboratory of Civil Engineering at Inonu University. These experimental studies were conducted as 10 series and illustrated in Table 3.7 in detail.

a) **Series 1:** Silty soil
b) **Series 2:** Silty soil reinforced with the natural crushed stones
c) **Series 3:** Silty soil reinforced with waste bricks
d) **Series 4:** Silty soil reinforced with recycled asphalt pavement
e) **Series 5:** Silty soil reinforced with natural crushed stones and encased with 25 cm height geogrid
f) **Series 6:** Silty soil reinforced with natural crushed stones and encased with 12.5 cm height geogrid
g) **Series 7:** Silty soil reinforced with waste bricks and encased with 25 cm height geogrid
h) **Series 8:** Silty soil reinforced with waste bricks and encased with 12.5 cm height geogrid

i) **Series 9:** Silty soil reinforced with recycled asphalt pavement and encased with 25 cm height geogrid

j) **Series 10:** Silty soil reinforced with recycled asphalt pavement and encased with 12.5 cm height geogrid

Ten laboratory experiments were conducted in total, with a circular steel model having a 5 cm diameter and a soil model with a height of 25 cm used for all tests. The height of the geogrid and the type of construction and demolition material were the variables in each experimental series. Table 3.7 contains five columns, which indicate the test number, testing serie, testing condition, D/df (tank diameter/foundation diameter), and water content of the silty soil, in that order.

Table 3.7. Experimental programme

Testing Serie	Testing condition	D/df	Water content of silty soil (%)
Series 1	Silty soil	5	32
Series 2	Silty soil reinforced with the natural crushed Stones	5	32
Series 3	Silty soil reinforced with waste bricks	5	32
Series 4	Silty soil reinforced with recycled asphalt pavement	5	32
Series 5	Silty soil reinforced with natural crushed stones and encased with 25 cm height geogrid	5	32
Series 6	Silty soil reinforced with natural crushed stones and encased with 12.5 cm height geogrid	5	32
Series 7	Silty soil reinforced with waste bricks and encased with 25 cm height geogrid	5	32
Series 8	Silty soil reinforced with waste bricks and encased with 12.5 cm height geogrid	5	32
Series 9	Silty soil reinforced with recycled asphalt pavement and encased with 25 cm height geogrid	5	32
Series 10	Silty soil reinforced with recycled asphalt pavement and encased with 12.5 cm height geogrid	5	32

3.4.1. Preparation of the silty soil sample

The silty soil was utilized to construct a soil foundation in the experimental series from 1 to 10. Initially, basic laboratory tests were carried out on the silty soil obtained from the field to determine its engineering properties. Samples with 32% water content were then prepared for use in laboratory tests. The reason for selecting 32% water content was to achieve a lower strength in terms of bearing capacity. During the preparation process, the samples obtained from the field were divided into smaller pieces and dried in an oven capable of providing a constant temperature of 105±5 °C for 24 hours. The samples were then ground using a grinding machine and sieved through a No. 10 sieve. Figure 3.22 provides a detailed view of the grinding equipment used.

Figure 3.22. Photo of the grinding machine used to grind silt

The dry samples grounded in a grinding machine was prepared with a water content of %32 and remolded with mixer until a homogenous water content was obtained. The prepared samples were replaced in transparent, air-free plastic cups. For the homogenous distribution, the samples were waited in a transparent, air-free plastic cups. The water content of the silty soil sample in the plastic cups was checked and maintained

at 32% before and after each test. Figure 3.23 illustrates the preservation of the silty soil in the plastic cups.

Figure 3.23. Photo of buckets used for storing silty soil

3.4.2. Preparation of the natural crushed stone sample

Series 2, Series 5, and Series 6 experiments involved the use of natural crushed stone for the stone column tests. Before the experiment, the natural crushed stone was washed and dried in an oven. The grain size of the natural crushed stone was chosen to align with the gradation curve. Figure 3.24 depicts the natural crushed stone that was prepared for the test.

Figure 3.24. Photo of the natural crushed stone used during the study

3.4.3. Preparation of the waste brick sample

Series 3, Series 7, and Series 8 experiments involved the use of waste brick for the stone column method. Waste brick was washed before the experiment and used after dried in the oven. The drain size of waste brick was selected to be in accordance with the gradation curve. The waste brick prepared for the test was illustrated in Figure 3.25.

Figure 3.25. Photo of the waste brick used during the study

3.4.4. Preparation of the recycled asphalt pavement sample

In Series 4, Series 9, and Series 10 experiments, Recycled asphalt pavement was used for stone column construction. recycled asphalt pavementwas washed before the experiment and used after dried in the oven. The drain size of recycled asphalt pavementwas selected to be in accordance with the gradation curve. The recycled asphalt pavementprepared for the test was illustrated in Figure 3.26.

Figure 3.26. Photo of the recycled asphalt pavement used during the study

3.4.5. Preparation of geogrid

In Series 5, 6, 7, 8, 9 and 10 experiments, geogrid was used for stone column construction. The geogrid sample cut from large roll was displayed in Figure 3.26 in detail. The geogrid was rolled up to be cylindrical shape and the head, middle, and the end edge was connected with a steel wire, where they come into contact with each other.

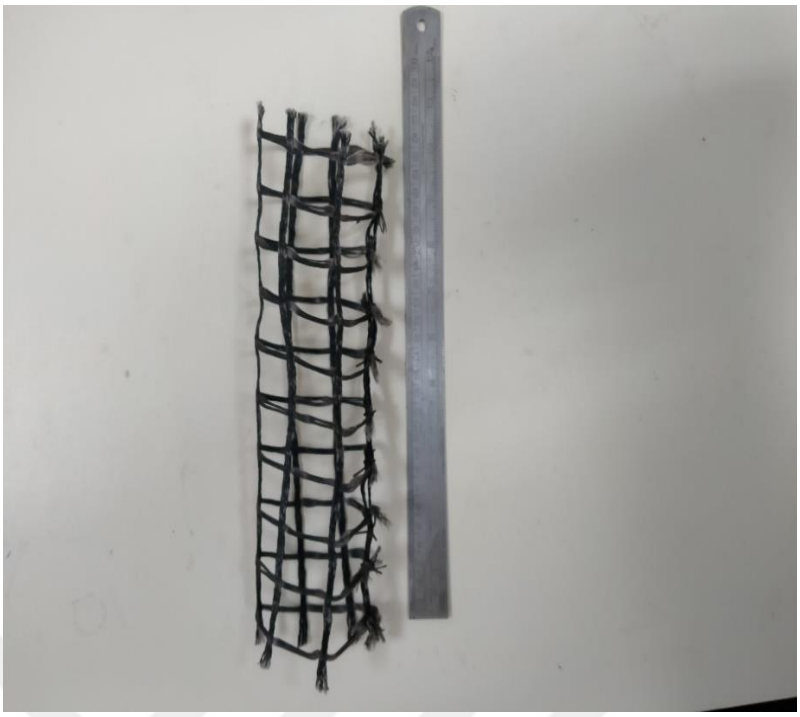

Figure 3.27. Photo of the ready geogrid sample used during the study

3.4.6. Series 1: Silty soil

During Series 1 plate loading test, the settlement-displacement behavior of the unreinforced silt soil on which the foundation sits was determined. The settlement-displacement behavior of the 5 cm diameter model foundation was examined in A, B, and C steel tanks with a diameter of 30 cm. The steel tanks were oiled before the test. The reason for this was to aim reducing the friction between them. The internal surface of the steel tank was marked with the slices of 5 cm to provide an easy homogenous settlement for silt soil. The level of silt soil inside the steel tank was determined to be 25 cm.

The method followed during the Series 1 experiments was outlined below:

1. The silty soil was replaced in the steel tank as 5 equal layers. The material amount per each layer was calculated from the equation given below.

$$\gamma_n = \frac{\gamma_s(1+w)}{(1+e)}$$

$$w = \gamma_n \times V$$

2. The silt soil with a water content of %32, which was controlled, was removed from transparent plastic cups, and weighed. The unit weight was calculated according to equation 3.1, and then it was placed in the steel tank. After the

placement was completed, the silty soil was compacted under a standard energy with the help of tamper.

3. Before starting the experiment, water content of the silt soil was checked to ensure if it was at the desired level. Water content samples were taken before and after the test for the silt soil with 32% water content. Strength control was performed with a hand penetrometer for every 5 cm layer of compacted soil, as shown in Figure 3.28.

Figure 3.28. Photo of strength control of silty soil with a hand penetrometer

4. After the components belonging to the plate loading system were placed, two displacement censors were located on the steel tank. In the experiment, the displacement-load readings were recorded using data logger, and the numerical values were transformed to a computer environment. Figure 3.29. illustrates the experimental set up for the silt soil with a water content of %32 placed in the tank with a diameter of 30 cm.

Figure 3.29. Photo of the experimental set-up from the series 1

3.4.7. Series 2: Silty soil reinforced with the natural crushed stones

In Series 2 of the plate loading test, it was conducted to investigate the bearing capacity of the silty soil when reinforced with natural crushed stone. The diameter of the stone column was 5 cm, and its height was 25 cm. The steel tanks and stone columns were aligned with each other, with their centers stacked on top of one another. The method followed during the Series 2 experiments was outlined below:

1. The silty soil amount of each layer was calculated according to Equation 3.1. formula. For each layer of 5 cm, it was compacted under a standard energy with the tamper.
2. Before the experiment, the stone column mold with a diameter of 5 cm was placed on the center of the empty steel tank. The lubricate was implemented to prevent adhesion between the silty soil and the stone column mold.
3. After the placement of stone column into steel tank, the silty soil sample was transferred to tank with 5 stages, totaling 25 cm.

4. Following the placement of silty soil sample with crushed stone, the samples were transferred into the stone column mold in 5 states with a total of 25 cm height, compacted using a tamper. Later, the stone column mold was slowly removed from the tank.
5. The model foundation was placed to cover up the entire surface of the stone column, and the loading was implemented. In the experiment, the displacement-load readings were recorded using data logger, and the numerical values were transformed to a computer environment. It was shown in detail in Figure 3.30.

Figure 3.30. Photo of the experimental set-up from the series 2

3.4.8. Series 3: Silty soil reinforced with waste bricks

During Series 3 experiments, the bearing capacity behavior of the silty soil was determined to improve or not by reinforcing it with waste bricks. The height of the stone column was 25 cm and diameter were 5 cm. The steel tanks and the stone columns were positioned in alignment with each other, with their centers stacked on top of each other. The method followed during the series 3 experiments was outlined below:

1. The silty soil amount of each layer was calculated according to Equation 3.1. formula. For each layer of 5 cm, it was compacted under a standard energy with the tamper.
2. Before the experiment, the stone column mold with a diameter of 5 cm was placed on the center of the empty steel tank. The lubricate was implemented to prevent adhesion between the silt soil and the stone column mold.
3. Following the placement stone column mold at the center of steel tank, silty soil sample was transferred into tank with 5 stages, to get a height of 25 cm.
4. After placing the silty soil sample and waste bricks, the samples were transferred into the stone column mold in 5 stages with a height of 25 cm, compacted using a tamper. Later, the stone column mold was slowly removed from the tank.
5. The model foundation was placed to cover up the entire surface of the stone column, and the loading was implemented. In the experiment, the displacement-load readings were recorded using data logger, and the numerical values were transformed to a computer environment. It was illustrated in Figure 3.31.

Figure 3.31. Photo of the experimental set-up from the series 3

3.4.9. Series 4: Silty soil reinforced with recycled asphalt pavement

During Series 4 experiments, the bearing capacity behavior of the silty soil was determined to improve by reinforcing the stone column with recycled asphalt pavement. The height of the stone column sample was 25 cm and the diameter was 5 cm. The steel tanks and the stone columns were positioned in alignment with each other, with their centers stacked on top of each other. The method followed during the Series 4 experiments was outlined below:

1. The amount of silty soil in each layer was calculated based on Equation 3.1. formula. For each layer, it was compacted under a standard energy with the tamper.
2. Before the experiment, the stone column mold with a diameter of 5 cm was placed on the center of the empty steel tank. The stone column mold placed in the center of the tank was lubricated.
3. Following the placement of stone column mold at the center of steel tank, the silty soil sample was transferred into tank in 5 stages, to get a height of 25 cm.
4. After placing the silt sample, the samples were transferred into the stone column mold in 5 stages with a total of 25 cm of recycled asphalt pavement, compacted using a tamper. Later, the stone column mold was slowly removed from the tank.
5. The model foundation was placed to cover up the entire surface of the stone column, and the loading was implemented. In the experiment, the displacement-load readings were recorded using data logger, and the numerical values were transformed to a computer environment. It was illustrated in Figure 3.32.

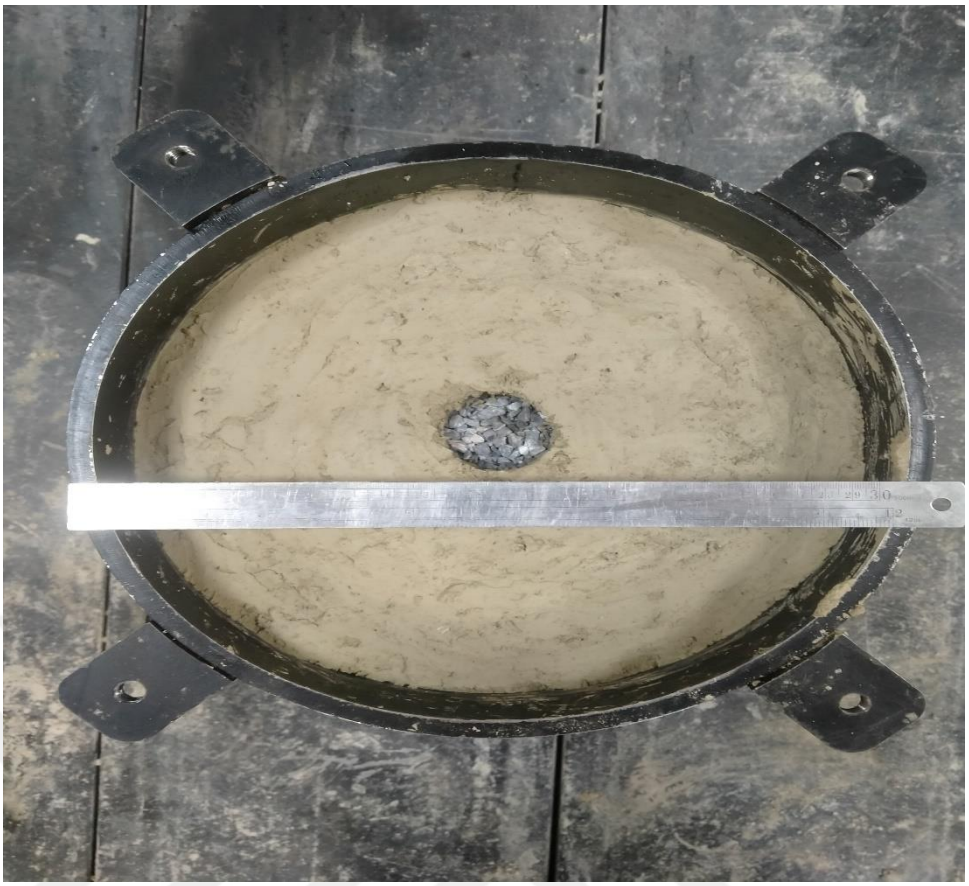

Figure 3.32. Photo of the experimental set-up from the series 4

3.4.10. Series 5: Silty soil reinforced with natural crushed stone and encased with 25 cm height geogrid

During series 5 experiments, the reinforcement of the silty soil with natural crushed stone using a geogrid encasement of 25 cm height will be determined in a 30 cm steel tank. The height of the stone column was determined to be 25 cm with a diameter of 5 cm in the experiment. The steel tanks and the geogrid encased stone columns were positioned in alignment with each other, with their centers stacked on top of each other.

The method followed during the series 5 experiments was outlined below:

1. As in the prior experiments, the amount of silt soil was placed into the steel tank in 5 stages based on Equation 3.1. formula. In each stage, a determined number of compaction processes were performed using the Standard Proctor Equipment.
2. The stone column mold was placed at the center of the steel tank, surrounded by a 360-degree encasement of geogrid material, with a height of 25 cm. The stone column mold placed in the center of the tank was lubricated.

3. The silty soil sample was evenly distributed into the steel tank in 5 layers.
4. After the placement of the silt soil, the natural crushed stone was placed into the stone column, and the construction of the geogrid-encased stone column with a height of 25 cm was completed.
5. Once the data from the experiments was transformed to computer environment, the experiment was concluded. It was illustrated in Figure 3.33 in detail.

Figure 3.33. Photo of the plate loading test from the series 5

3.4.11. Series 6: Silty soil reinforced with natural crushed stone and encased with 12.5 cm height geogrid

During series 6 experiments, the reinforcement of the silty soil with natural crushed stone using a geogrid encasement of 12.5 cm height will be determined in a 30 cm steel tank. The height of the stone column was determined to be 25 cm with a diameter

of 5 cm in the experiment. The steel tanks and the geogrid encased stone columns were positioned in alignment with each other, with their centers stacked on top of each other.

The method followed during the series 6 experiments was outlined below:

1. The amount of silty soil was placed into the steel tank in 5 stages, totaling 12.5 cm in height based on Equation 3.1. In each stage, a determined number of compaction processes were performed using the Standard Proctor Device.
2. The stone column mold was placed at the center of the steel tank, surrounded by the encasement of geogrid material, with a height of 12.5 cm. The stone column mold placed in the center of the tank was lubricated.
3. The silty sample was evenly distributed into the steel tank in 5 layers.
4. After the placement of the silt soil, the natural crushed stone was placed into the stone column, and the construction of the geogrid-encased stone column with a height of 12.5 cm was completed.
5. Once the data in the process of test was obtained from the data logger, the experiment was completed.

3.4.12. Series 7: Silty soil reinforced with waste bricks and encased with 25 cm height geogrid

During series 7 experiments, the reinforcement of the silty soil with waste brick using a geogrid encasement of 25 cm height will be determined in a 30 cm steel tank. The height of the stone column was determined to be 25 cm with a diameter of 5 cm in the experiment. The steel tanks and the geogrid encased stone columns were positioned in alignment with each other, with their centers stacked on top of each other.

The method followed during the series 7 experiments was outlined below:

1. According to Equation 3.1, the amount of silt soil was placed into the steel tank in 5 stages, to get a height of 25 cm. In each stage, a determined number of compaction processes were performed using the standard proctor equipment.
2. The stone column mold was placed at the center of the steel tank, surrounded by the encasement of geogrid material, with a height of 25 cm. The stone column mold placed in the center of the tank was lubricated.
3. The silty soil sample was evenly distributed into the steel tank in 5 layers.

4. After the placement of the silt soil, the waste brick was placed into the stone column, and the construction of the geogrid-encased stone column with a height of 25 cm was completed.
5. Once the data in the process of test was obtained from the data logger, the experiment was completed.

3.4.13. Series 8: Silty soil reinforced with waste bricks and encased with 12.5 cm height geogrid

During series 8 experiments, the reinforcement of the silty soil with waste brick using a geogrid encasement of 12.5 cm height will be determined in a 30 cm steel tank. The height of the stone column was determined to be 25 cm with a diameter of 5 cm in the experiment. The steel tanks and the stone columns were positioned in alignment with each other, with their centers stacked on top of each other.

The method followed during the series 8 experiments was outlined below:

1. The silty soil amount of each layer was calculated according to Equation 3.1. formula. For each layer of 5 cm, it was compacted under a standard energy with the tamper.
2. Before the experiment, the stone column mold with a diameter of 5 cm was placed on the center of the empty steel tank. The lubricate was implemented to prevent adhesion between the silt soil and the stone column mold.
3. Following the placement of stone column mold at the center of steel tank, the silty soil sample with a height of 12.5 cm was transferred into tank with 5 stages.
4. After placing the silt sample, the samples were transferred into the stone column mold in 5 stages with a total of 12.5 cm of waste brick, compacted using a tamper, and later the stone column was slowly removed.
5. The model foundation was placed to cover up the entire surface of the stone column, and the loading was implemented. In the experiment, the displacement-load readings were recorded using data logger, and the numerical values were transformed to a computer environment.

3.4.14. Series 9: Silty soil reinforced with recycled asphalt pavement and encased with 25 cm height geogrid

During series 9 experiments, the reinforcement of the silty soil with recycled asphaly pavement using a geogrid encasement of 25 cm height will be determined in a 30 cm steel tank. The height of the stone column was determined to be 25 cm with a diameter of 5 cm in the experiment. The steel tanks and the geogrid encased stone columns were positioned in alignment with each other, with their centers stacked on top of each other.

The method followed during the series 9 experiments was outlined below:

1. According to Equation 3.1, the amount of silt soil was placed into the steel tank in 5 stages, totaling 25 cm. In each stage, a determined number of compaction processes were performed using the Standard proctor device.
2. The stone column mold was placed at the center of the steel tank, surrounded by the encasement of geogrid material, with a height of 25 cm. The stone column mold placed in the center of the tank was lubricated.
3. The silt sample was evenly distributed into the steel tank in 5 layers.
4. After the placement of the silt soil, the natural crushed stone was placed into the stone column, and the construction of the geogrid-encased stone column with a height of 25 cm was completed.
5. Once the data in the process of test was obtained from the data logger, the experiment was completed.

3.4.15. Series 10: Silty soil reinforced with recycled asphalt pavement and encased with 12.5 cm height geogrid

During series 9 experiments, the reinforcement of the silty soil with recycled asphaly pavement using a geogrid encasement of 12.5 cm height will be determined in a 30 cm steel tank. The height of the stone column was determined to be 25 cm with a diameter of 5 cm in the experiment. The steel tanks and the geogrid encased stone columns were positioned in alignment with each other, with their centers stacked on top of each other.

The method followed during the series 10 experiments was outlined below:

1. According to Equation 3.1, the amount of silt soil was placed into the steel tank in 5 stages, totaling 25 cm. In each stage, a determined number of compaction processes were performed using the Standard proctor device.

2. The stone column mold was placed at the center of the steel tank, surrounded by the encasement of geogrid material, with a height of 12.5 cm. The stone column mold placed in the center of the tank was lubricated.
3. The silty soil sample was evenly distributed into the steel tank in 5 layers.
4. After the placement of the silt soil, the recycled asphalt pavementwas placed into the stone column, and the construction of the geogrid-encased stone column with a height of 12.5 cm was completed.
5. Once the data in the process of test was obtained from the data logger, the experiment was completed.

3.5. Application of Numerical Analyses

The PLAXIS finite element method was preferred for the numerical analysis throughout the thesis. The program was currently used in the field of geotechnical engineering to determine soil properties such as bearing capacity, consolidation, stress-strain behavior, and etc. Due to the experimental set-up, axisymmetric model was preferred in the numerical analysis. Mohr Coulomb (MC) was selected to model natural crushed stone, recycled asphalt pavement, and waste brick materials used in the stone column method. The parameters required for modeling were the dilation angle (ψ), internal friction angle (ϕ), cohesion (C_{ref}), Poisson's ratio (v), elastic modulus (E_{ref}), and saturated unit weight and unsaturated unit weight (γ_{sat} and γ_{unsat}). The parameters used in in the numerical analysis for the silty soil are displayed in Table 3.8.

Table 3.8. Modelling parameters of the silty soil

Parameter	Value
Water content (%)	32
Unit weight (kN/m^3)	18.54
Cohesion (c_{ref}) (kPa)	42
Young's modulus (kPa) (E_{ref})	385
Poisson's ratio (v)	0.35
Internal angle of friction (ϕ)	1
Dilation angle (ψ)	0

The parameters for used for the modelling the natural crushed stone are illustrated in Table 3.9

Table 3.9. Modelling parameters of the natural crushed stone

Parameter	Value
Cohesion (c_{ref}) (kPa)	1.56
Young's Modulus (kPa) (E_{ref})	61000
Poisson's Ratio (v)	0.3
Internal Friction Angle (ϕ)	47.81
Dilation Angle (ψ)	17.81

The parameters for waste brick used during the modelling of the stone column samples are shown in Table 3.10.

Table 3.10. Modelling parameters of the waste brick

Parameter	Value
Cohesion ($c_{ref)}$ (kPa)	14.68
Young's Modulus (kPa) (E_{ref})	60000
Poisson's Ratio (v)	0.3
Internal Friction Angle (ϕ)	41.03
Dilation Angle (ψ)	11.03

The parameters for recycled asphalt pavement used during the modelling of the stone column are illustrated in Table 3.11.

Table 3.11. Modelling parameters of the recycled asphalt pavement

Parameter	Value
Cohesion (c_{ref}) (kPa)	9.92
Young's Modulus (kPa) (E_{ref})	59000
Poisson's Ratio (v)	0.3
Internal Friction Angle (ϕ)	39.48
Dilation Angle (ψ)	9.48

3.5.1. Series 1: Numerical analysis of silty soil

The data used in the experimental studies was utilized in the numerical analyses of series 1. The steel tank with a diameter of 30 cm was used in the analyses.

The method followed during the series 1 experiments was outlined below:

1. Axisymmetric model was selected from the setting tab.
2. The construction elements were drawn by the "Line" command.

3. The opened window with "Show Materials" command defined the parameters used for the silt soil through the saturated and unsaturated unit weight (γ_{sat} and γ_{unsat}), the internal friction angle (ϕ), and cohesion (c_{ref}).
4. Figure 3.34 illustrates The PLAXIS 2D Model for analysis number 1.

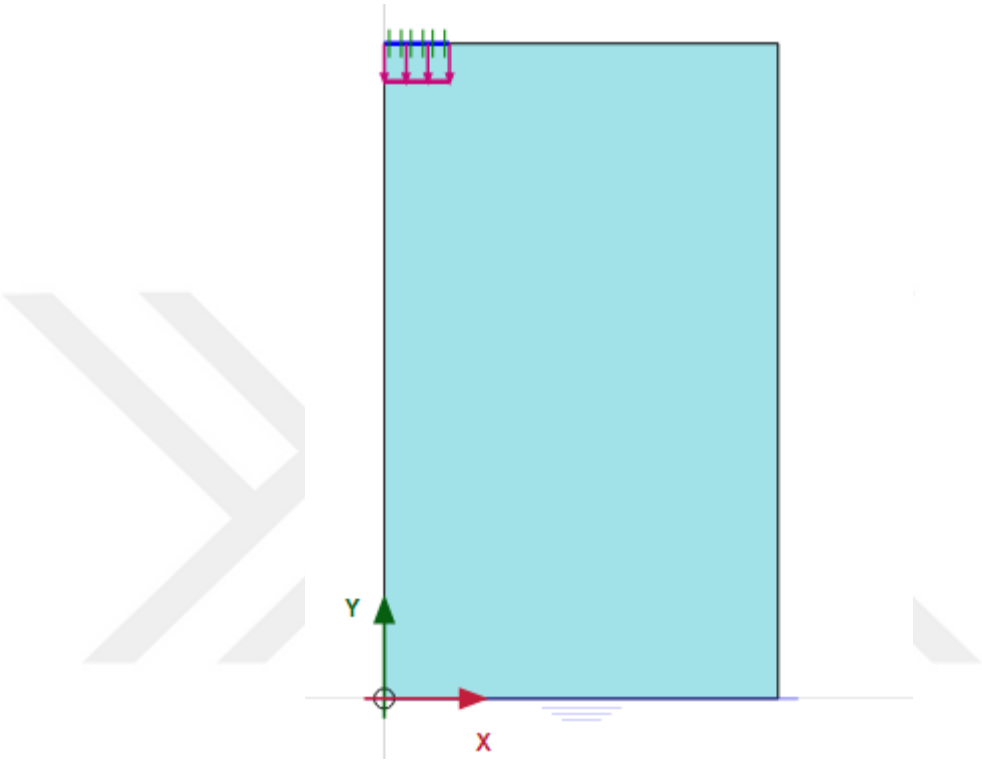

Figure 3.34. PLAXIS 2D model for the numerical analysis series 1

5. The model was transformed into finite element mesh with the "mesh" command. It was displayed in Figure 3.35.

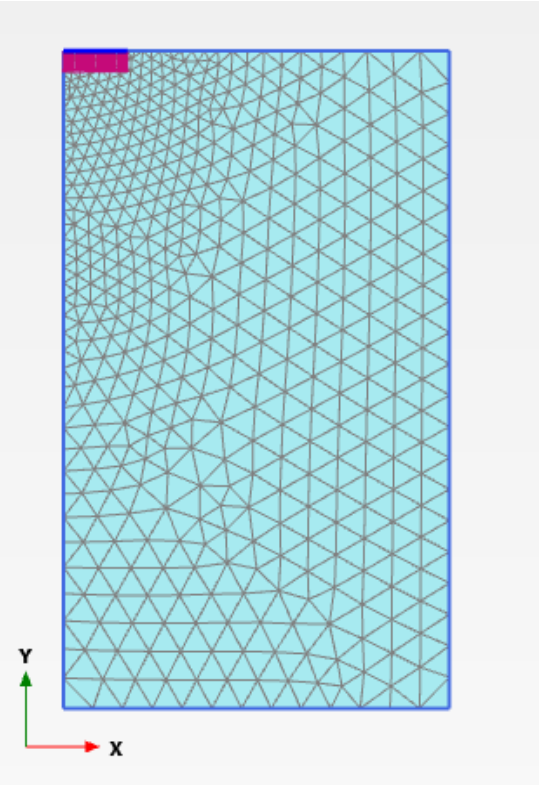

Figure 3.35. Mesh definition for the numerical analysis series 1

6. The controls were respectively conducted through "Flow Conditions" tab.
7. "Select points for curves" command was used from the "Staged Construction" tab to select Node 1, the top left corner of the model foundation.
8. The analysis was started by using "Calculate" command.
9. After the end of analysis, the load-displacement graphs were created with using "Curves" command. Later, the load-displacement values were created in the form of numbers and transformed into numerical values by using "Table" command. This can be seen on Figure 3.36.

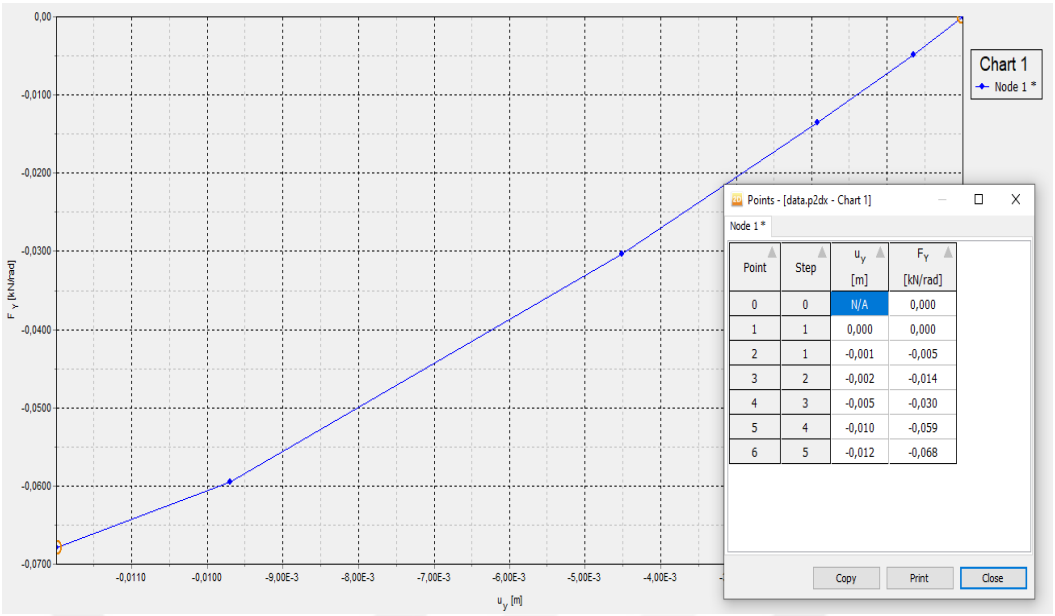

Figure 3.36 Graph and table results for the load (F_y) and vertical displacement (U_y) in analysis number 1

3.5.2. Series 2: Numerical analysis of silty soil reinforced with natural crushed stones

In the numerical analysis of series 2, the same steps and procedures used in Series 1 was applied. As a difference, the natural crushed stone material and its properties was added through the window opened with "Show Materials" command. Furthermore, the stone column mold was added from the "structures" tab, and its properties was entered. The model prepared with PLAXIS 2D for analysis number 2 was displayed in Figure 3.37.

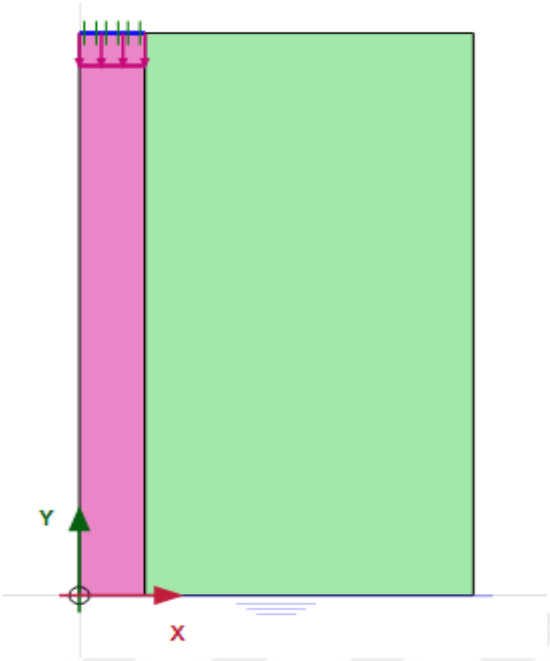

Figure 3.37. PLAXIS 2D model for the numerical analysis series 2

As a result of the analyses of series 2, the total displacement in the axis Uy was illustrated in 3.38.

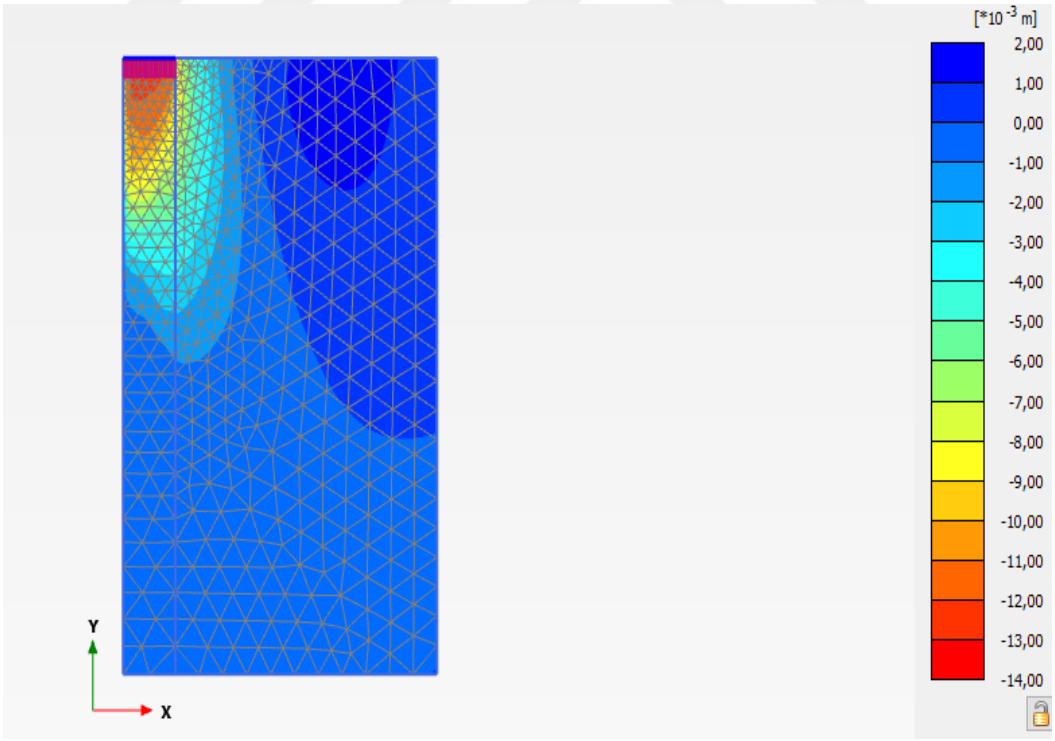

Figure 3.38. Total displacement for the numerical analysis series 2

The load- displacement graphs was drawn and transformed into numerical values with the "Table" command. This is demonstrated in Figure 3.39.

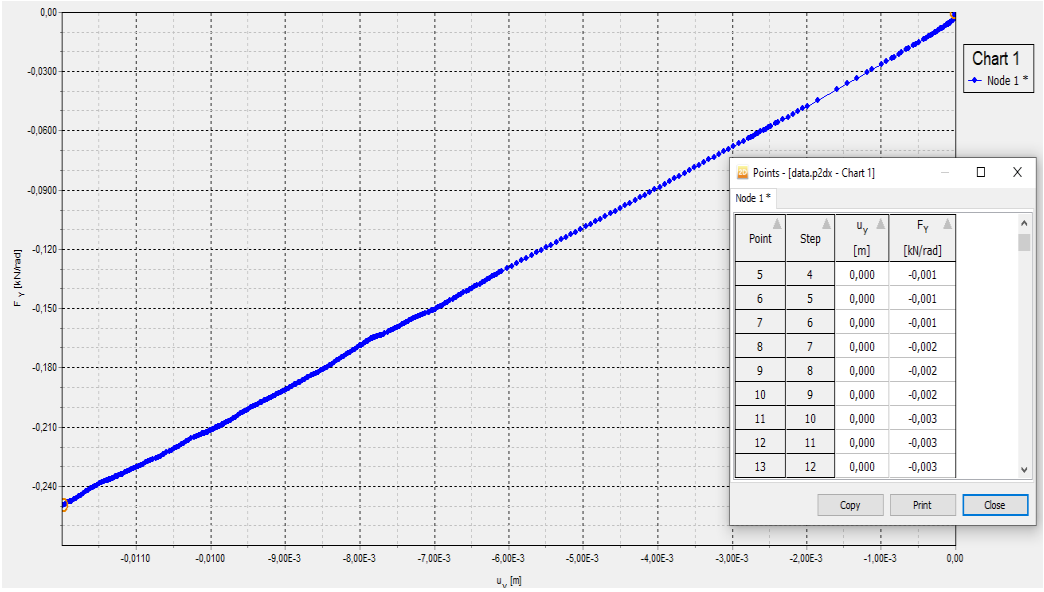

Figure 3.39 Graph and table results for the load (F_y) and vertical displacement (U_y) in analysis number 2

3.5.3. Series 3: Numerical analysis of silty soil reinforced with waste bricks

In the numerical analysis of Series 3, the same steps and procedures used in Series 2 was applied. As a difference, the waste brick material and its properties were added through the window opened with "Show Materials" command. The displacement was transformed into the finite element mesh by using the "mesh" command, illustrated in Figure 3.40.

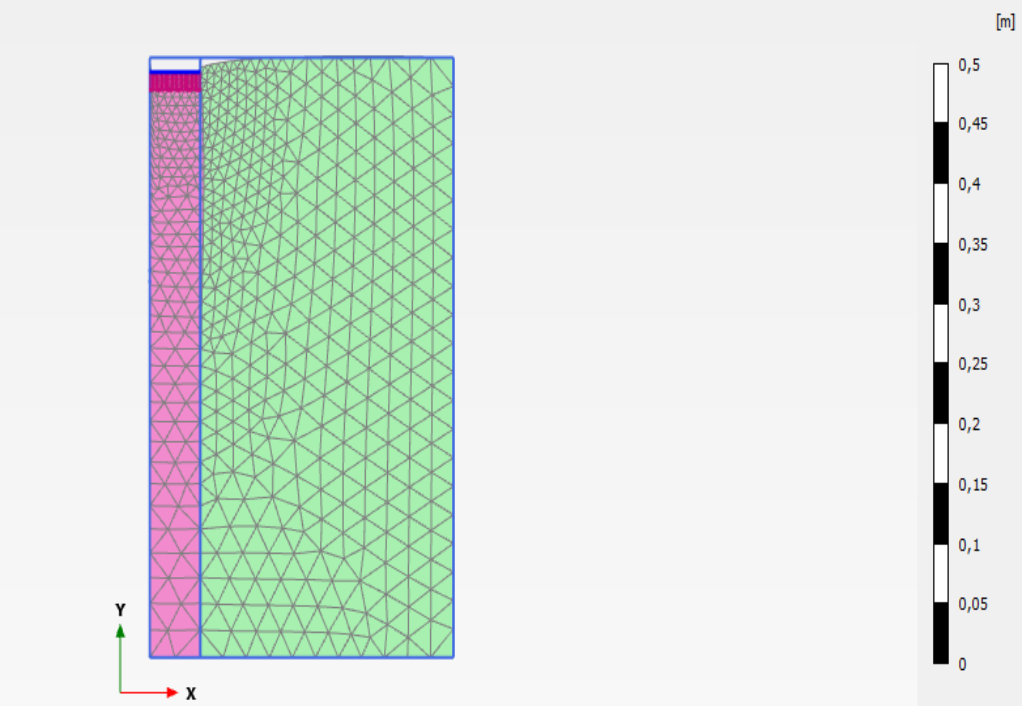

Figure 3.40. Deformed mesh for the numerical analysis series 3

3.5.4. Series 4: Numerical analysis of silty soil reinforced with recycled asphalt pavement

In the numerical analysis of series 4, the same steps and procedures used in series 2 was applied. As a difference, the recycled asphalt pavement material and its properties were added through the window opened with "Show Materials" command. As a result of the numerical analyses of series 4, the total displacement is presented in Figure 3.41.

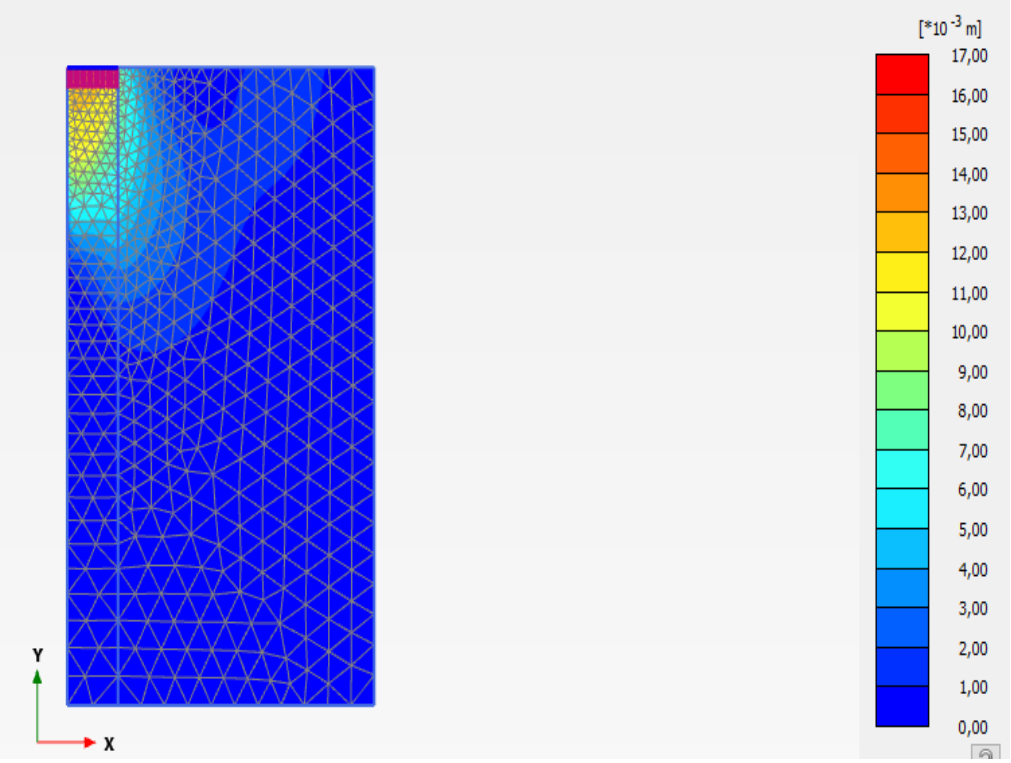

Figure 3.41. Total displacement for the numerical analysis series 4

The load- displacement graphs was drawn and transformed into numerical values with the "Table" command. This can be seen in Figure 3.42.

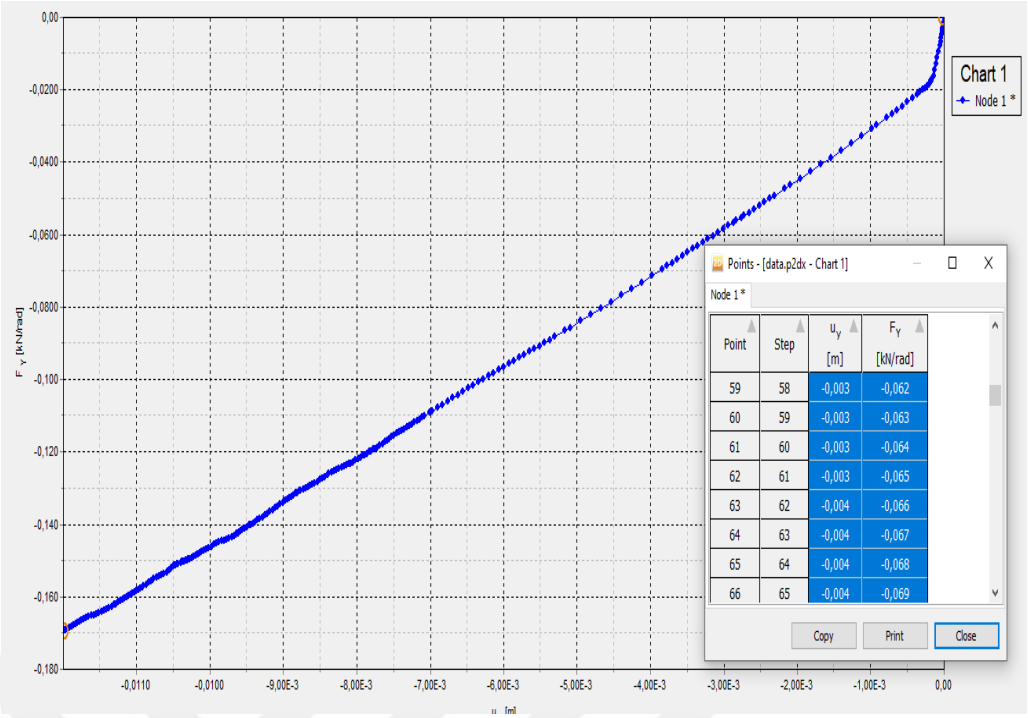

Figure 3.42. Graph and table results for the load (F_y) and vertical displacement (U_y) in analysis number 4

3.5.5. Series 5: Numerical analysis of silty soil reinforced with natural crushed stones and encased with 25 cm height geogrid

During the numerical analyses of series 5, the geogrid-encased stone column mold with a height of 25 cm was inserted into the silty soil with a water content of %32. The steel tank diameter was preferred to be 30 cm. The same method was used during the examination of numerical analysis in series 2. The model prepared with PLAXIS 2D for analysis number 5 is displayed in Figure 3.43.

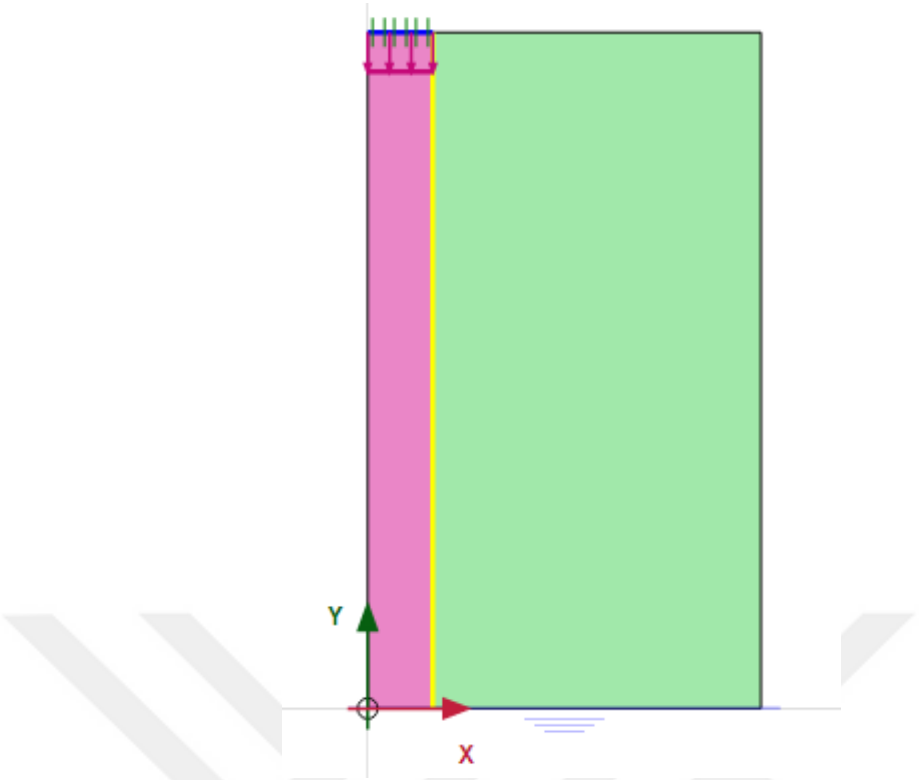

Figure 3.43. PLAXIS 2D model for the numerical analysis series 5

As a result of the numerical analyses of series 5, the total displacement is presented in Figure 3.44.

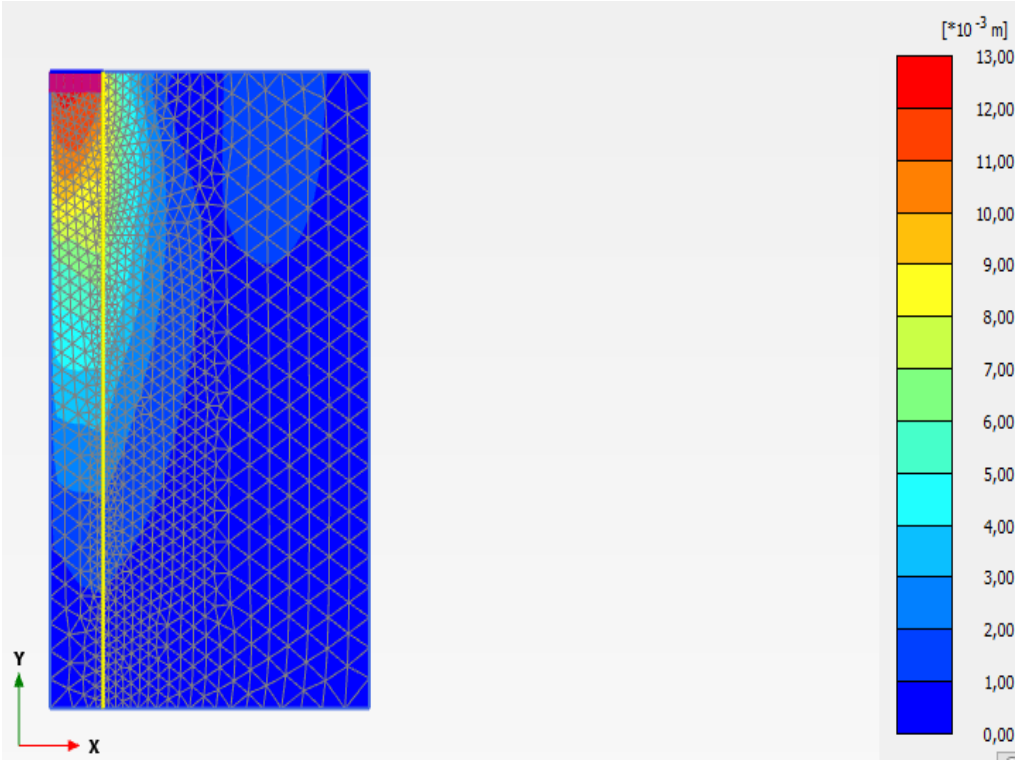

Figure 3.44. The total displacement for the numerical analysis series 5

The load- displacement graph was drawn and transformed into numerical values with the "Table" command and is displayed in Figure 3.45.

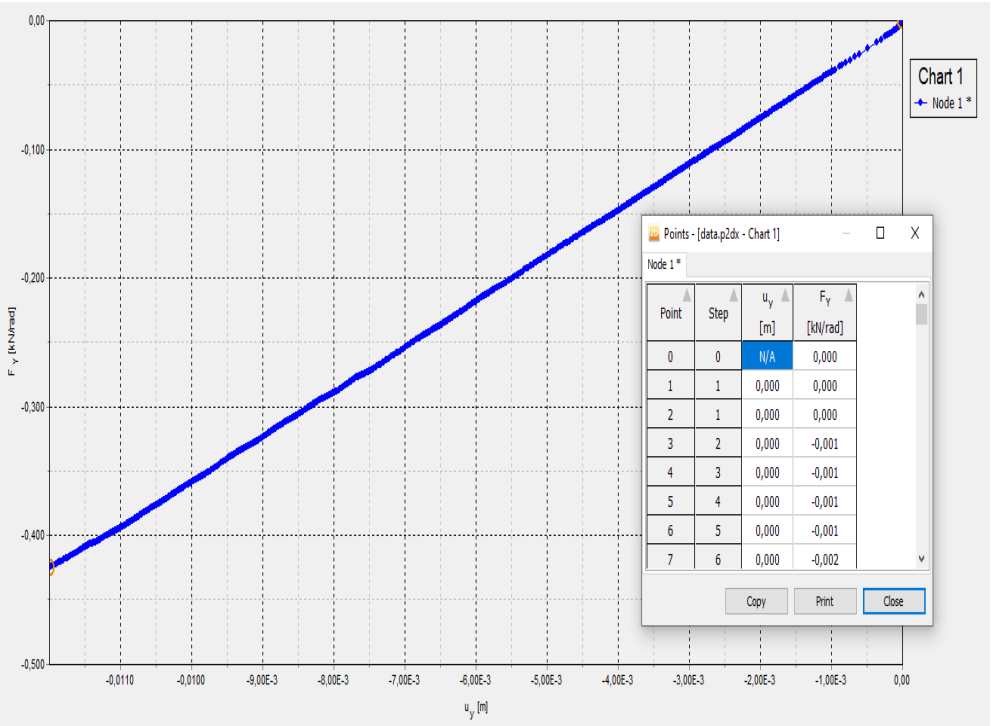

Figure 3.45. Graph and table results for the load (F_y) and vertical displacement (U_y) in analysis number 1

3.5.6. Series 6: Numerical analysis of silty soil reinforced with natural crushed stones and encased with 12.5 cm height geogrid

During the numerical analyses of series 6, the geogrid-encased stone column mold with a height of 12.5 cm was inserted into the silt soil with a water content of %32. In the numerical analysis of series 5, the same steps and procedures was applied. As a difference, the modeling of the geogrid-encased stone column with a height of 12.5 cm was performed. Figure 3.46 illustrates the PLAXIS 2D model for analysis number 6.

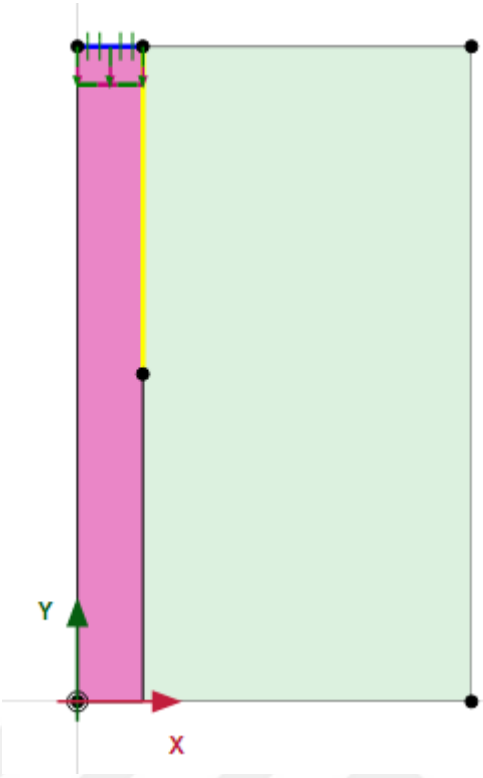

Figure 3.46. PLAXIS 2D model for the numerical analysis series 6

The model was transformed into finite element mesh with the "mesh" command. This can be seen on Figure 3.47.

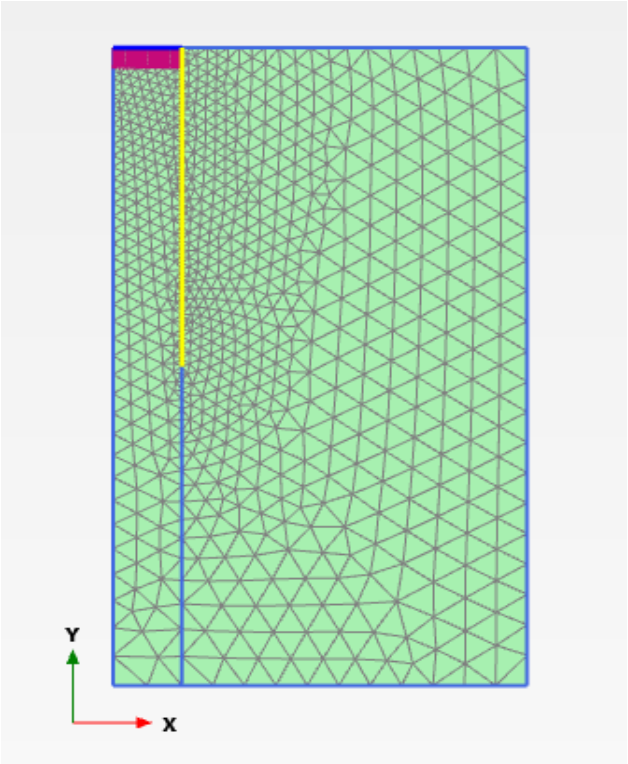

Figure 3.47. Mesh definition for the numerical analysis series 6

As a result of the numerical analyses of series 6, the total displacement is presented in Figure 3.48.

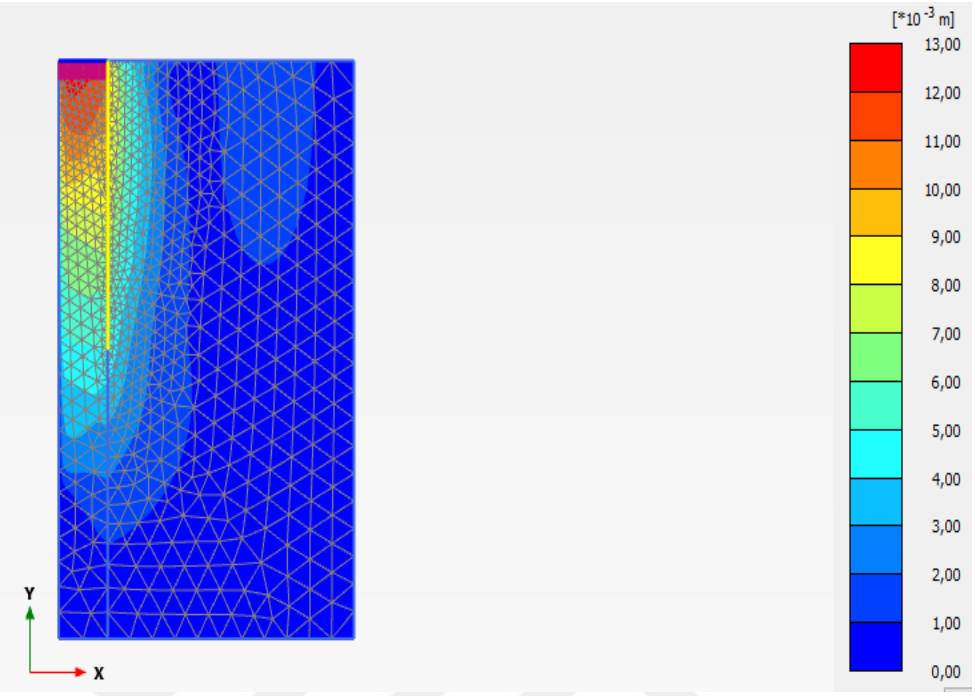

Figure 3.48. Total displacement for analysis number 6

The load- displacement graph was drawn and transformed into numerical values with the "table" command. This is shown on Figure 3.49.

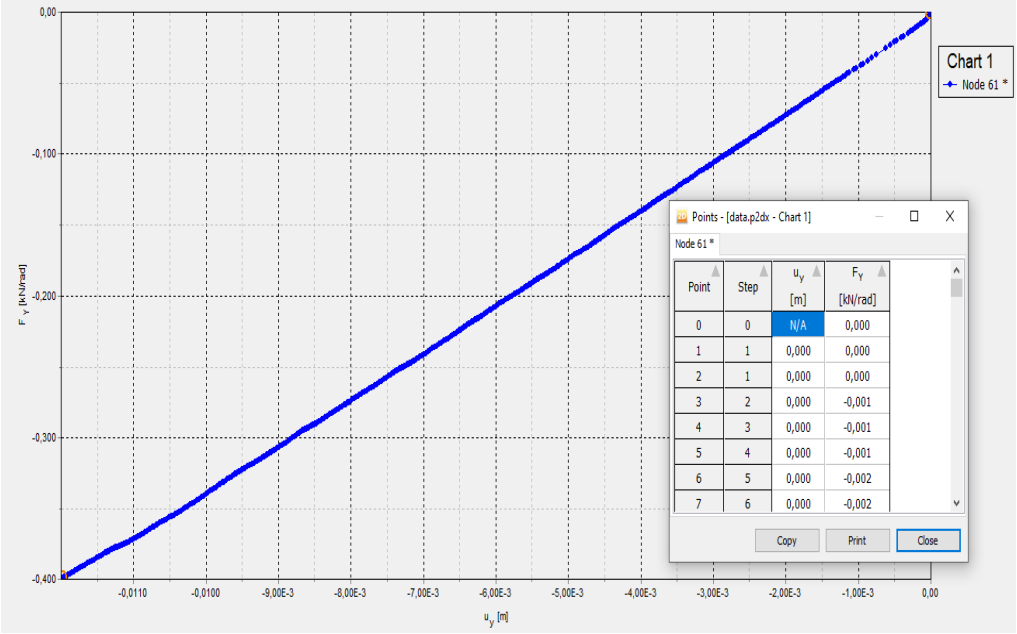

Figure 3.49. Graph and table results for the load (F_y) and vertical displacement (U_y) in analysis number 6

3.5.7. Series 7: Numerical analysis of silty soil reinforced with waste bricks and encased with 25 cm height geogrid

In the numerical analysis of series 7, the same steps and procedures used in series 5 was applied. As a difference, the waste brick was inserted to the stone column rather than natural crushed stone. The model was transformed into finite element mesh with the "mesh" command and the mesh can be seen in Figure 3.50.

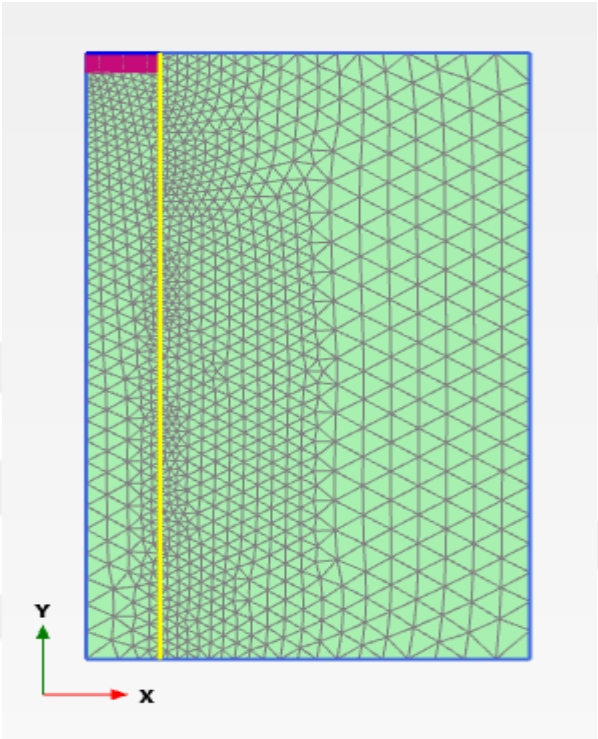

Figure 3.50. Mesh definition for the numerical analysis series 7

In this numerical analysis, the point selection for displacement-load is shown in detail in Figure 3.51, with the coordinates (0,25).

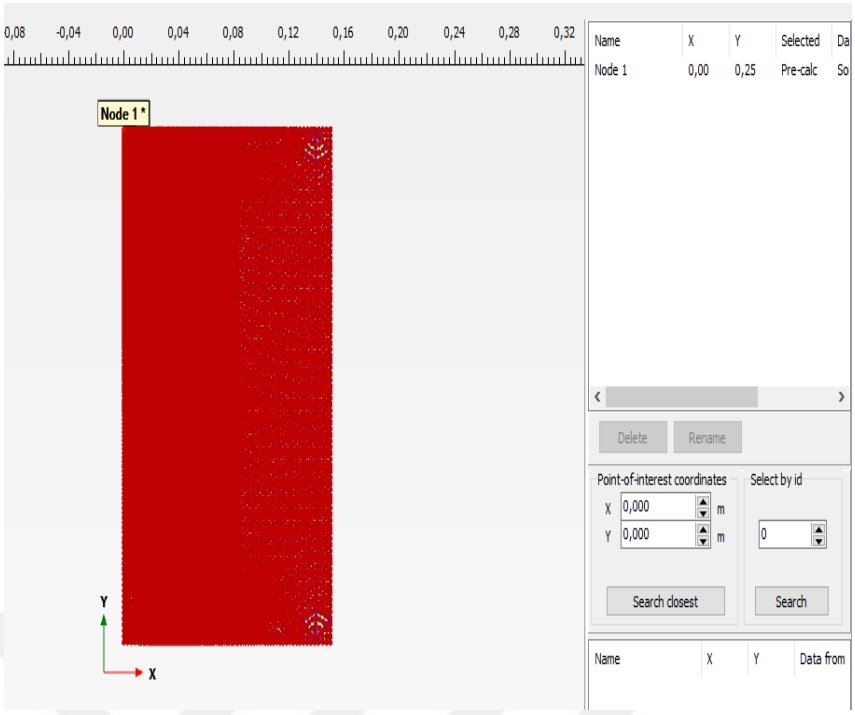

Figure 3.51. Point selection for the numerical analysis series 7

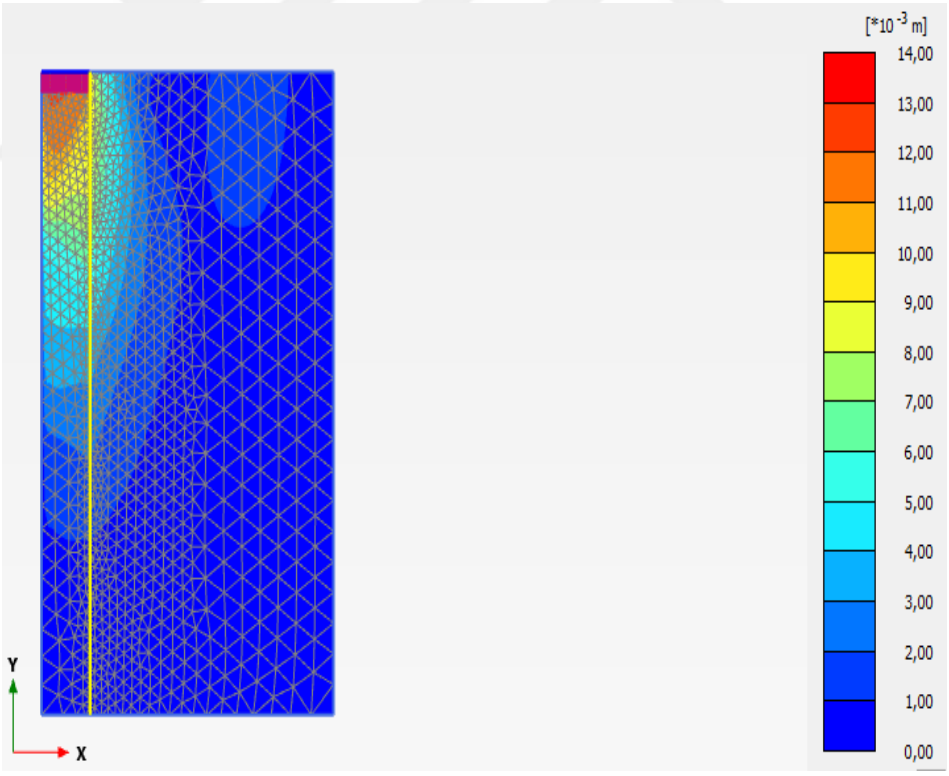

Figure 3.52. Total displacement for the numerical analysis series 2

The load- displacement graph was drawn and transformed into numerical values with the "table" command and is illustrated in Figure 3.53.

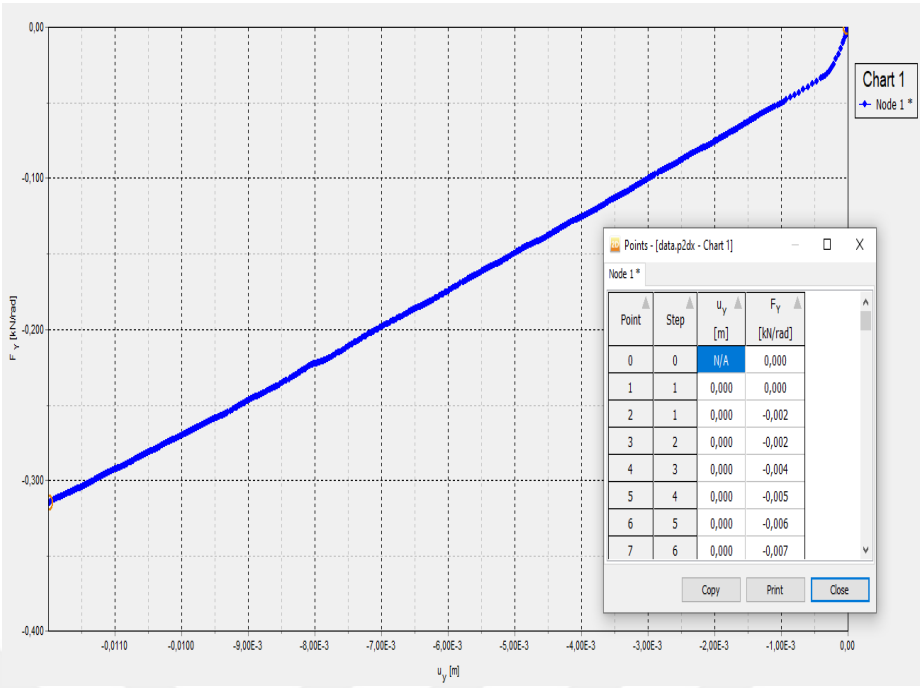

Figure 3.53. Graph and table results for the load (F_y) and vertical displacement (U_y) in analysis number 7

3.5.8 Series 8: Numerical analysis of silty soil reinforced with waste bricks and encased with 12.5 cm height geogrid

In the numerical analysis of series 8, the same steps and procedures used in series 7 was applied. As a difference, the modeling of the geogrid-encased stone column with a height of 12.5 cm was performed. The PLAXIS 2D Model for analysis number 8 was prepared. The model was transformed into finite element mesh with the "mesh" command and is displayed in Figure 3.54.

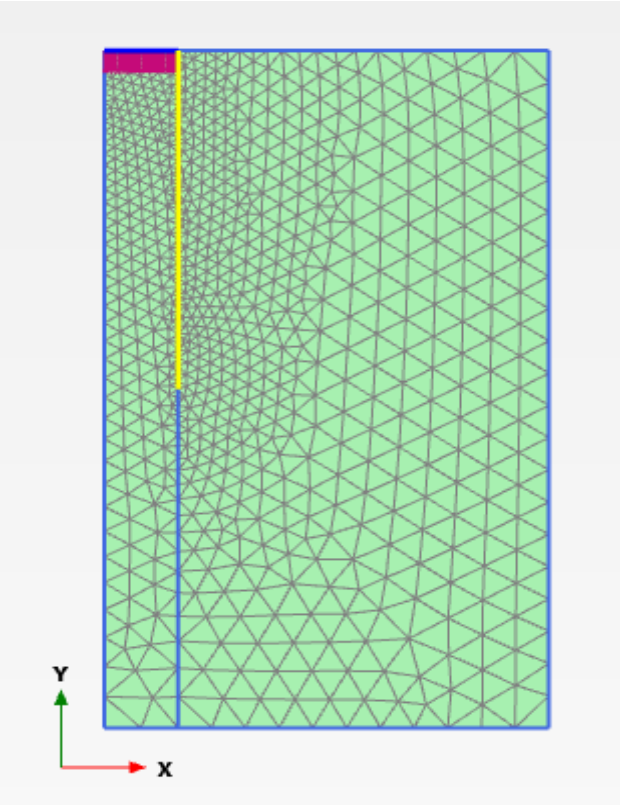

Figure 3.54. Mesh definition for the numerical analysis series 8

As a result of the numerical analyses of series 8, the total displacement is presented in Figure 3.55.

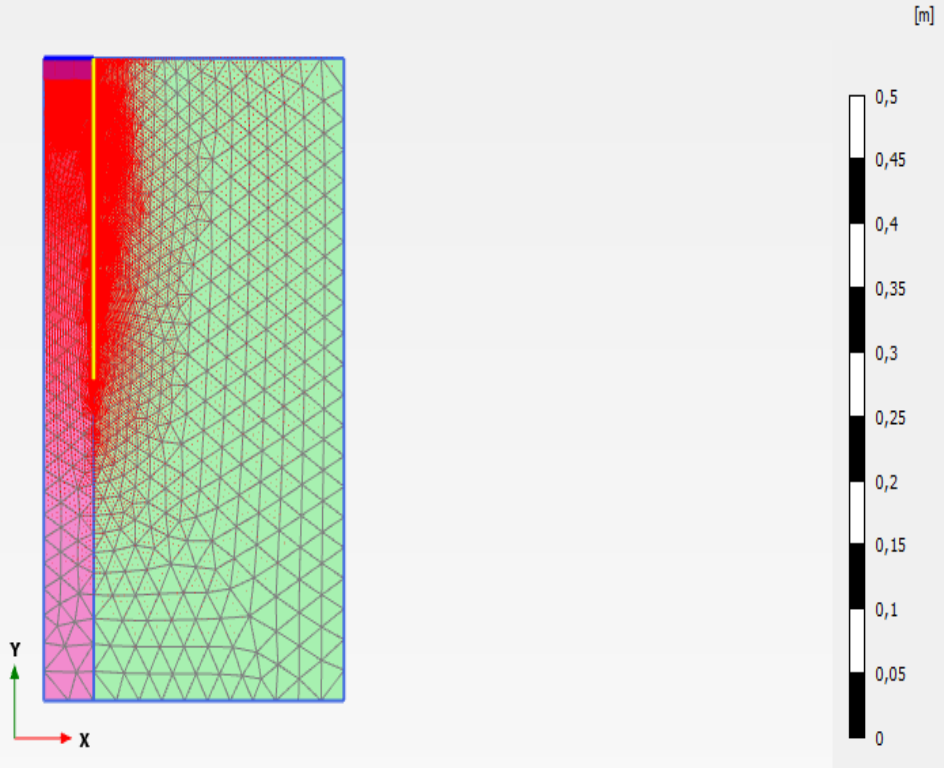

Figure 3.55. Total displacement for the numerical analysis series 8

. The load-displacement graph was drawn and transformed into numerical value, as shown in Figure 3.56.

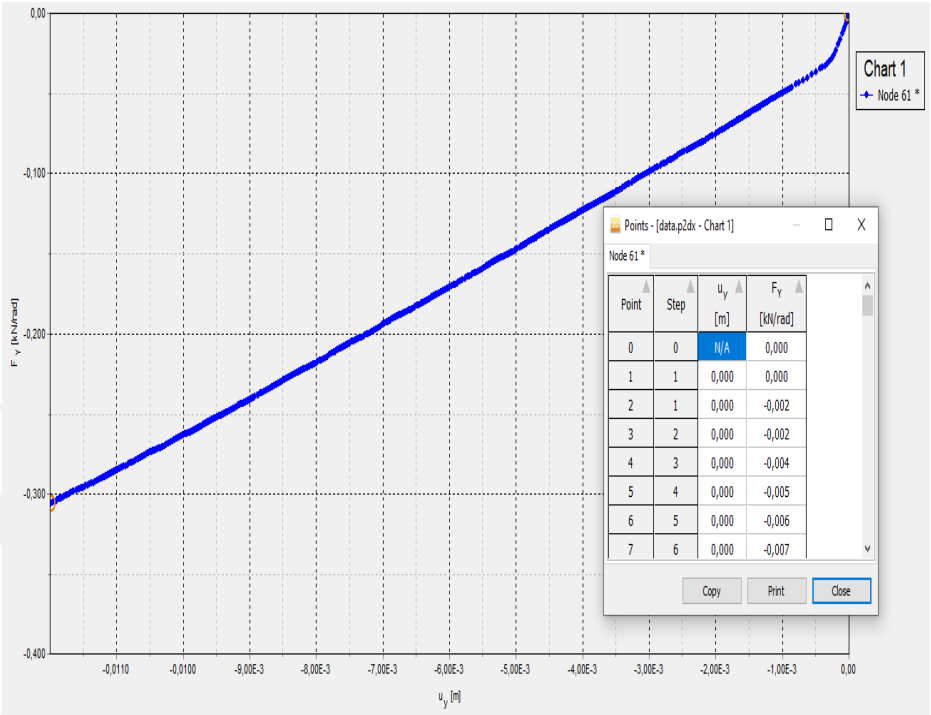

Figure 3.56. Graph and table results for the load (F_y) and vertical displacement (U_y) in analysis number 8

3.5.9. Series 9: Numerical analysis of silty soil reinforced with recycled asphalt pavement and encased with 25 cm height geogrid

In the numerical analysis of series 9, the same steps and procedures used in series 7 was applied. As a difference, the recycled asphalt pavement material was inserted into the stone column rather than waste brick. The model was transformed into finite element mesh with the "mesh" command. As a result of the numerical analyses of series 9, the total displacement is presented in Figure 3.57.

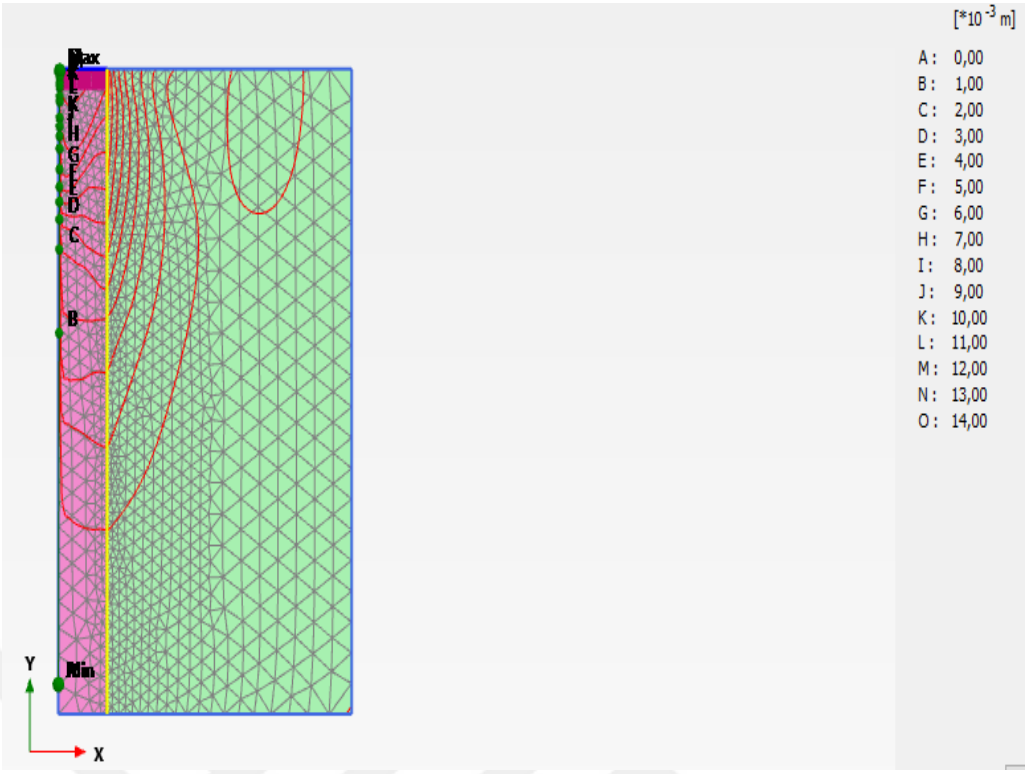

Figure 3.57. Total displacement for the numerical analysis series 9

The load- displacement graph was drawn and transformed into numerical values with the "table" command and is displayed in Figure 3.58.

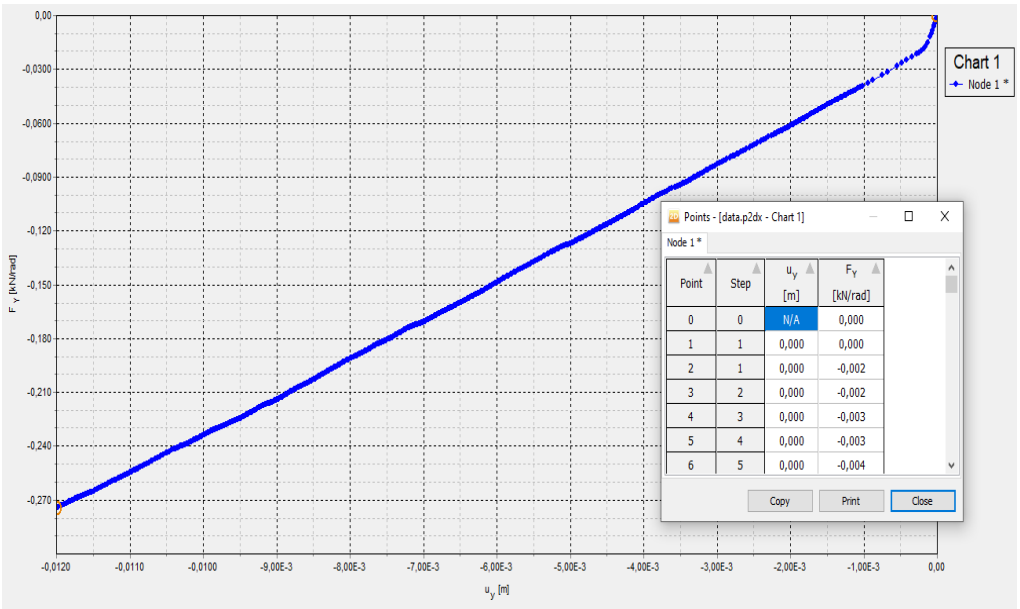

Figure 3.58. Graph and table results for the force (F_y) and vertical displacement (U_y) in analysis number 9

3.5.10. Series 10: Numerical analysis of silty soil reinforced with recycled asphalt pavement and encased with 12.5 cm height geogrid

In the numerical analysis of series 10, the same steps and procedures used in Series 9 was applied. As a difference, the modeling of the geogrid-encased stone column with a length of 12.5 cm was performed. The PLAXIS 2D Model for analysis number 10 was prepared. The model was transformed into finite element mesh with the "mesh" command. As a result of the numerical analyses of series 10, the total displacement is presented in Figure 3.59.

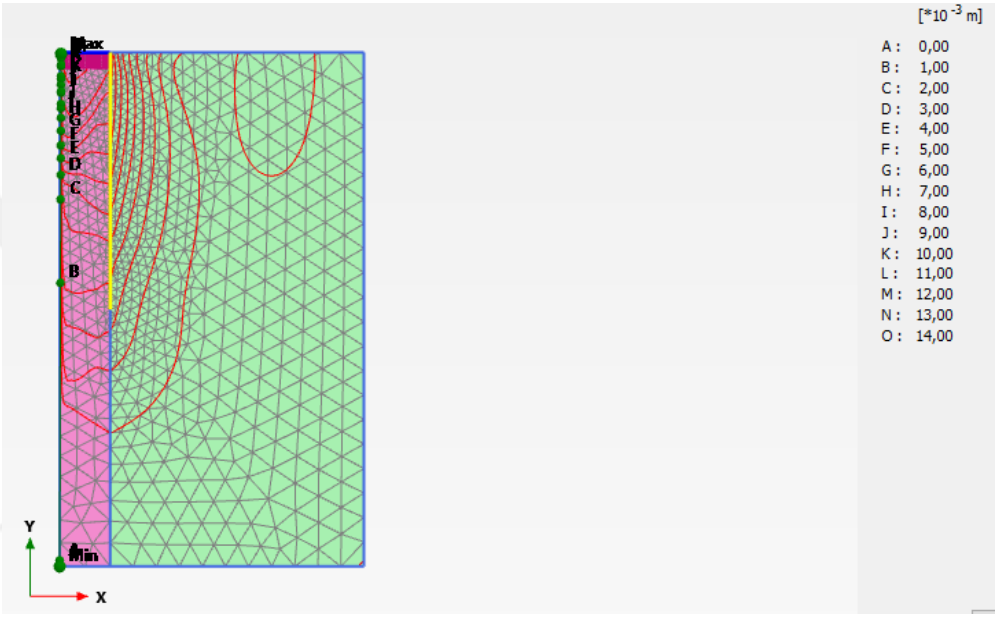

Figure 3.59. Total displacement for the numerical analysis series 10

The load- displacement graph was drawn and transformed into numerical values with the "table" command and is demonstrated in Figure 3.60.

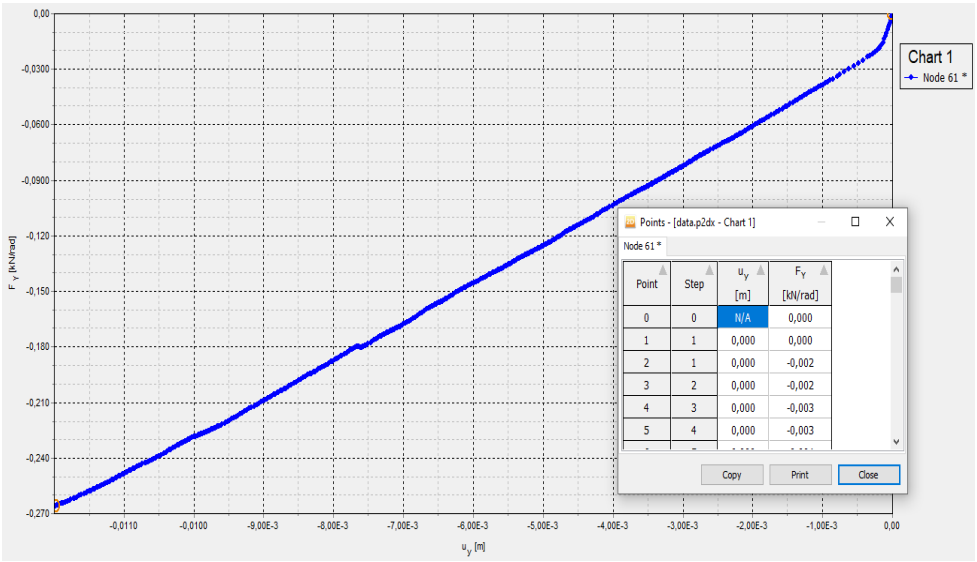

Figure 3.60. Graph and table results for the load (F_y) and vertical displacement (U_y) in analysis number 10

4. RESULTS AND DISCUSSION

The findings of this study were evaluated by commenting on the results obtained from both the experimental study and the numerical analyses. The obtained results were evaluated as figures and tables.

4.1. Findings Obtained from the Experimental Results

In the experimental study, a total of ten sequential experiments were conducted. The experiments listed below were conducted in the laboratory environment: Series 1: The experiment in the case of unreinforced silt soil, Series 2: The experiment in the case of the silty soil reinforced with natural crushed stone, Series 3: The experiment in the case of silty soil reinforced with waste bricks, Series 4: The experiment in the case of silty soil reinforced with recycled asphalt pavement, Series 5: The experiment in the case of silty soil reinforced with natural crushed stone and using a geogrid encasement of 25 cm height, Series 6: The experiment in the case of silty soil reinforced with natural crushed stone and using a geogrid encasement of 12.5 cm height, Series 7: The experiment in the case of silty soil reinforced with waste brick and using a geogrid encasement of 25 cm height, Series 8: The experiment in the case of silty soil reinforced with waste brick and using a geogrid encasement of 12.5 cm height, Series 9: The experiment in the case of silty soil reinforced with recycled asphalt pavement and using a geogrid encasement of 25 cm height, Series 10: The experiment in the case of silty soil reinforced with recycled asphalt pavement and using a geogrid encasement of 12.5 cm height. In this section, the experimental series were evaluated in the form of graphs and tables

During the experiment series, the model foundation with a diameter of 5 cm and %32 water content was compared. The results were examined in graphs form. In the graphs, the vertical axis shows the applied stress (bearing capacity) in units of kPa, while the horizontal axis represents the settlement ratio s/d (%) as a percentage. The stress values which occurred at settlement values corresponding to 10% of the foundation diameter.

4.1.1. Comparison of the results in series 1, 2, 3 and 4

The bearing capacity of the experiment series corresponding to %10 settlement ratio with %32 water content was displayed in Figure 4.1. The bearing capacity results

were determined in this order: Series-1 107.92 kPa, Series-2 398.44 kPa, Series-3 384.82 kPa and Series-4 284.52 kPa.

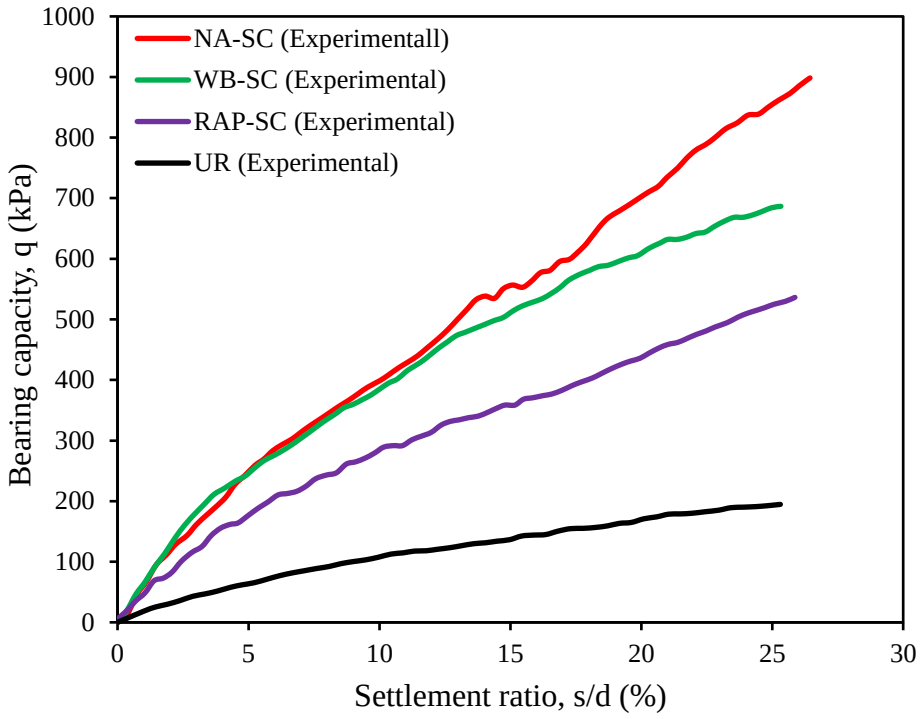

Figure 4.1. Bearing capacity-settlement ratio curves for the experimental series 1, 2, 3 and 4

4.1.2. Comparison of the results in series 1, 2, 5 and 6

The comparison of all testing results conducted with natural crushed stone was performed in the experiment series 1, 2, 5 and 6. During this experimental series, the model foundation with a diameter of 5 cm and %32 water content have been compared. The value of the bearing capacity equaling to %10 settlement ratio were evaluated.

In Figure 4.2, the bearing capacity of the experimental series for the silty soil with %32 water content was determined respectively series-1 107.92 kPa, series-2 398.44 kPa, series-5 645.95 kPa and series-6 624.08 kPa.

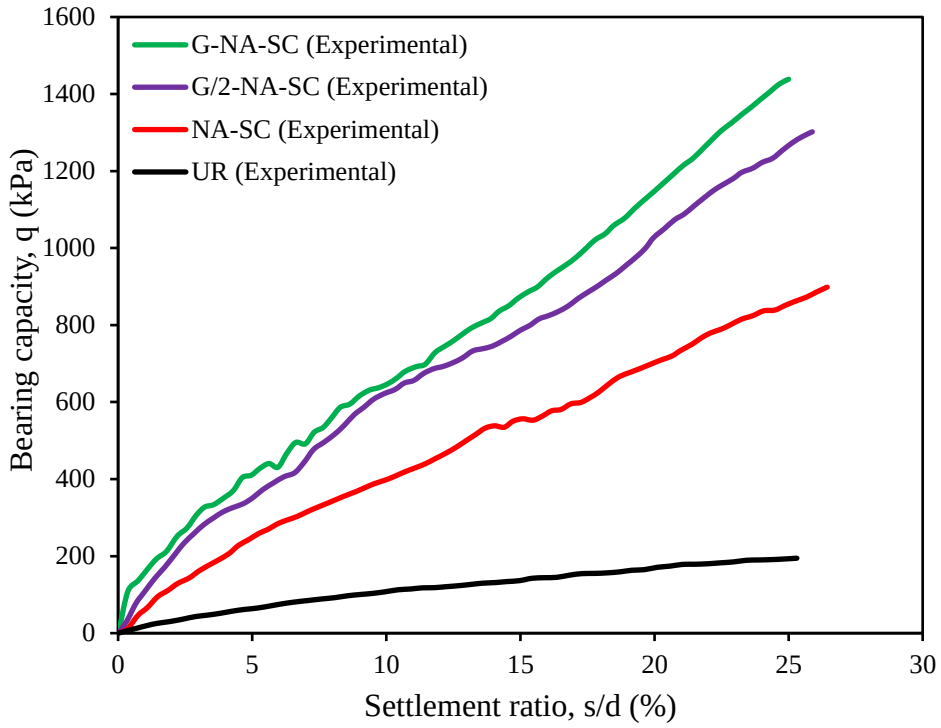

Figure 4.2. Bearing capacity-settlement ratio curves for the experimental series 1, 2, 5 and 6

4.1.3. Comparison of the results in series 1, 3, 7 and 8

The comparison of all tests conducted with waste brick was performed in the experimental series 1, 3, 7 and 8. The comparison was made between the experiments conducted with the model foundation of 5 cm diameter and a water content of 32%. The value of the bearing capacity equaling to %10 settlement ratio was evaluated.

The results of experimental series were shown in Figure 4.3. The bearing capacity of the experimental series were determined to be respectively series-1 107.92 kPa, series-3 384.82 kPa, series-7 597.51 kPa, and series-8 552.57 kPa.

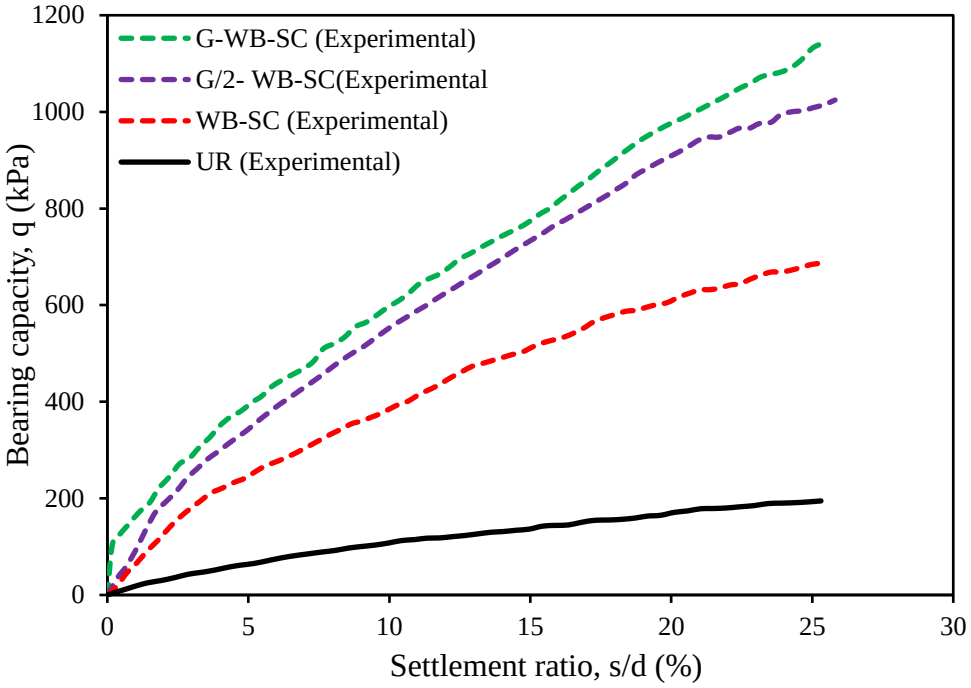

Figure 4.3. Bearing capacity-settlement ratio curves for the experimental series 1, 3, 7 and 8

4.1.4. Comparison of the results in series 1, 4, 9 and 10

The comparison of all tests conducted with recycled asphalt pavement was performed in the experimental series 1, 4, 9 and 10. Comparison was made between the experiments conducted with a steel tank of 30 cm diameter and a model foundation of 5 cm diameter, with a water content of 32%. The value of the bearing capacity equaling to %10 settlement ratio was read. The bearing capacities were shown in detail in Figure 4.4.

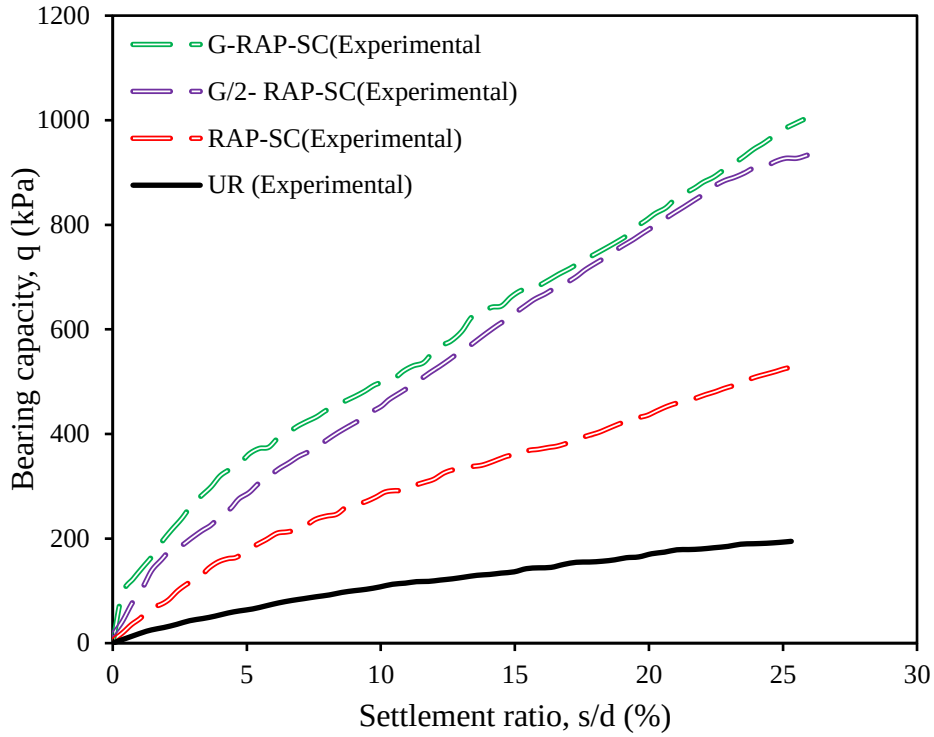

Figure 4.4. Bearing capacity-settlement ratio curves for the experimental series 1, 4, 9 and 10

The results of experimental series were shown in Figure 4.4. The bearing capacity of the experiment series was found to be respectively series-1 107.92 kPa, series-4 284.52 kPa, series-9 497.63 kPa, and series-10 452.57 kPa.

4.1.5. Comparison of the results in series 1, 5, 7 and 9

Comparison was made among all the experiments conducted with stone column constructions using geogrid of 25 cm height in this test series. The experiments were conducted with a water content of %32, using a steel tank of 30 cm diameter and a model foundation of 5 cm diameter for comparison.

The findings of the experiment were analyzed in Figure 4.5. The bearing capacity of the experimental series were determined to be series-1 107.92 kPa, series-5 645.95 kPa, series-7 597.51 kPa, and series-9 497.63 kPa.

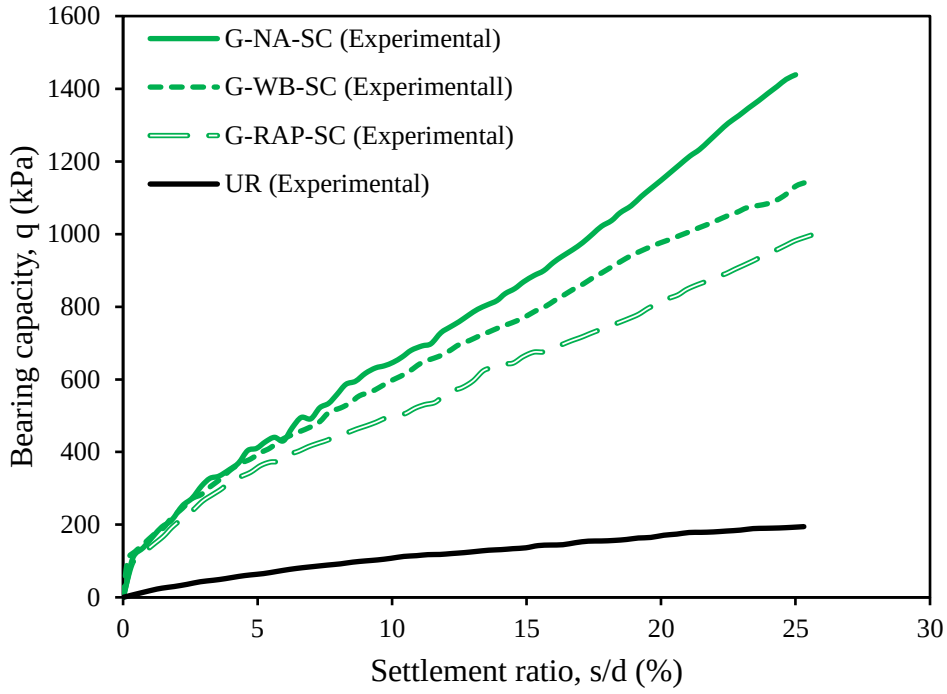

Figure 4.5. Bearing capacity-settlement ratio curves for the experimental series 1, 5, 7 and 9

4.1.6. Comparison of the results in series 1, 6, 8 and 10

Comparison was made among all the experiments conducted with stone column constructions using geogrid of 12.5 cm in height in the test series. The comparison was made between the experiments conducted with the model foundation of 5 cm diameter and a water content of 32%. The value of stress was the bearing capacity equaling to %10 settlement ratio.

The experiment results were examined in Figure 4.6. The bearing capacity of the experiment series was determined to be respectively series-1 107.92 kPa, series-6 624.08 kPa, series-8 552.57 kPa, and series-10 452.57 kPa.

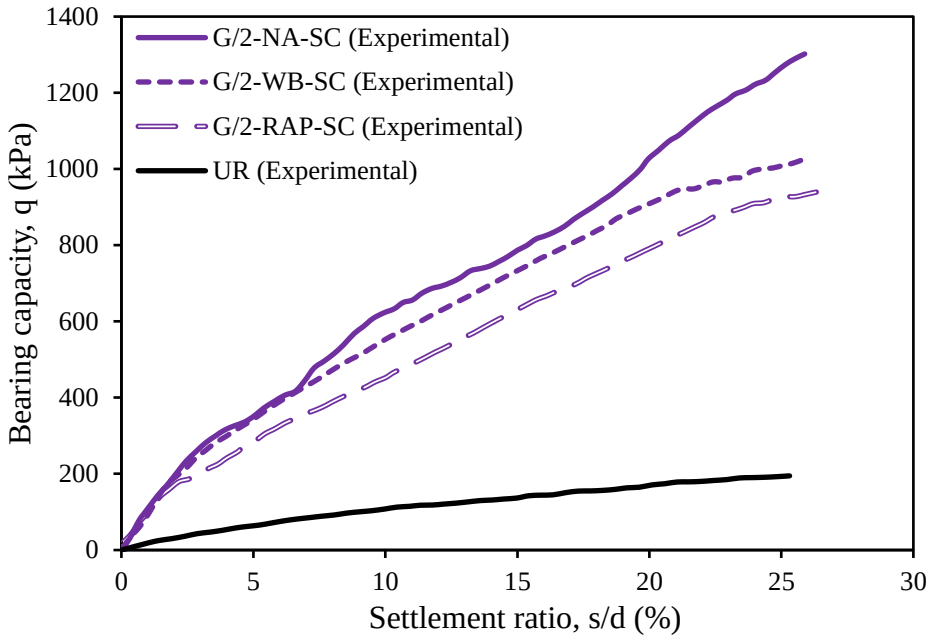

Figure 4.6. Bearing capacity-settlement ratio curves for the experimental series 1, 6, 8 and 10

4.2. Findings Obtained From the Numerical Analyses

As a result of the experimental studies conducted in the Geotechnic Laboratory, the findings were modelled by Plaxis Software, a finite element method, and numerical analyses were applied.

The numerical analyses were conducted as 10 series. The analyses were displayed in a graph and tables form. According to the results obtained from the numerical analyses, the sudden changes were found to be less compared to the experimental studies.

4.2.1. Comparison of the numerical analyses in series 1, 2, 3 and 4

Numerical analysis was performed to compare the stone column samples using silty soil, natural crushed stone, waste brick and recycled asphalt pavement materials. The numerical analyses were compared with the experimental series using the same diameter model foundation and %32 water content. The value of bearing capacity read from the graphs represents stress value corresponding to %10 settlement ratio.

In Figure 4.7, the bearing capacity of the numerical analysis was found respectively to be series-1 106.42 kPa, series-2 351.44 kPa, series-3 327.53 kPa and series-4 271.58 kPa.

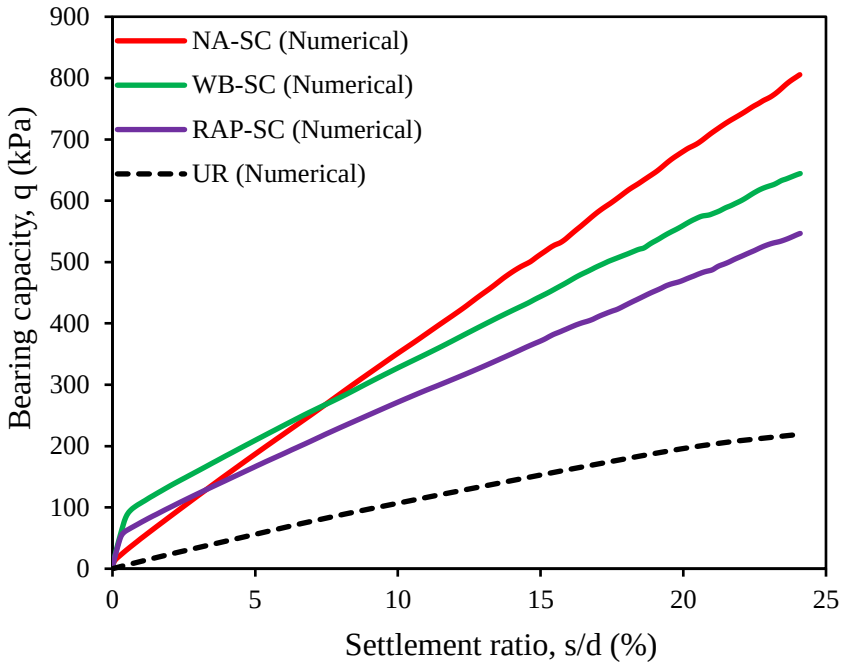

Figure 4.7. Bearing capacity-settlement ratio curves for the numerical series 1, 2, 3 and 4

4.2.2. Comparison of the numerical analyses in series 1, 2, 5 and 6

The comparison of all tests conducted with natural crushed stone was conducted in the numerical analyses of experiment Series. The numerical analyses were compared with the experimental series using the model foundation with 5 cm diameter and %32 water content. The value of stress was the bearing capacity equaling to %10 settlement ratio.

In Figure 4.8., the bearing capacity of the numerical analysis was found respectively to be series-1 106.42 kPa, series-2 351.44 kPa, series-5 586.29 kPa and series-6 559.71 kPa.

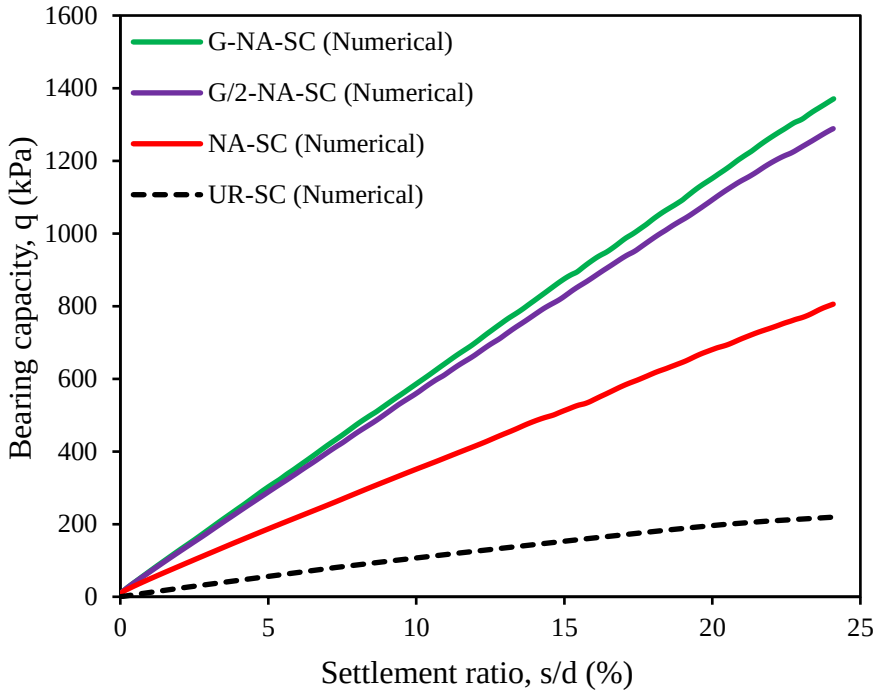

Figure 4.8. Bearing capacity-settlement ratio curves for the numerical series 1, 2, 5 and 6

4.2.3. Comparison of the numerical analyses in series 1, 3, 7 and 8

The numerical analyses were compared for the construction of stone columns using waste brick, 25 cm length geogrid, and 12.5 cm length geogrid. The numerical analyses were compared with the experimental series using the model foundation with 5 cm diameter and %32 water content. The value of stress was the bearing capacity equaling to %10 settlement ratio.

In Figure 4.9, the bearing capacity of the numerical analysis was found respectively to be series-1 106.42 kPa, series-3 327.53 kPa, series-7 481.61 kPa ve series-6 474.31 kPa.

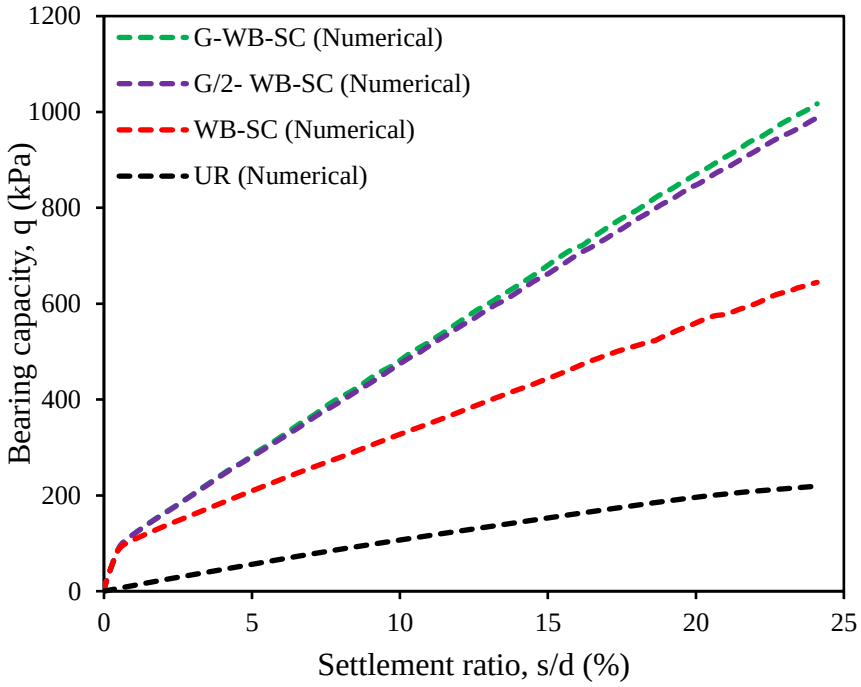

Figure 4.9. Bearing capacity-settlement ratio curves for the numerical series 1, 3, 7 and 8

4.2.4. Comparison of the numerical analyses in series 1, 4, 9 and 10

The numerical analyses were compared for the construction of stone columns using recycled asphalt pavement, 25 cm length and 12.5 cm length geogrid. The numerical analyses were compared with the experimental series using the model foundation with 5 cm diameter and %32 water content.

The value of stress was the bearing capacity equaling to %10 settlement ratio.

In Figure 4.10, the bearing capacity of the numerical analysis was found respectively to be series-1 106.42 kPa, series-4 271.58 kPa, series-9 408.93 kPa and series-10 403.43 kPa.

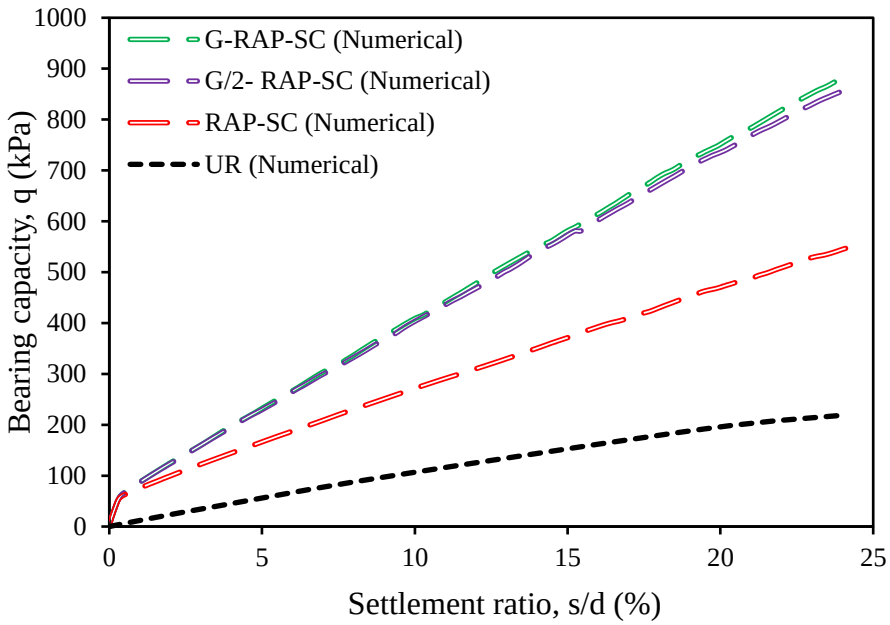

Figure 4.10. Bearing capacity-settlement ratio curves for the numerical series 1, 4, 9 and 10

4.3. Comparison of the Numerical and Experimental Results

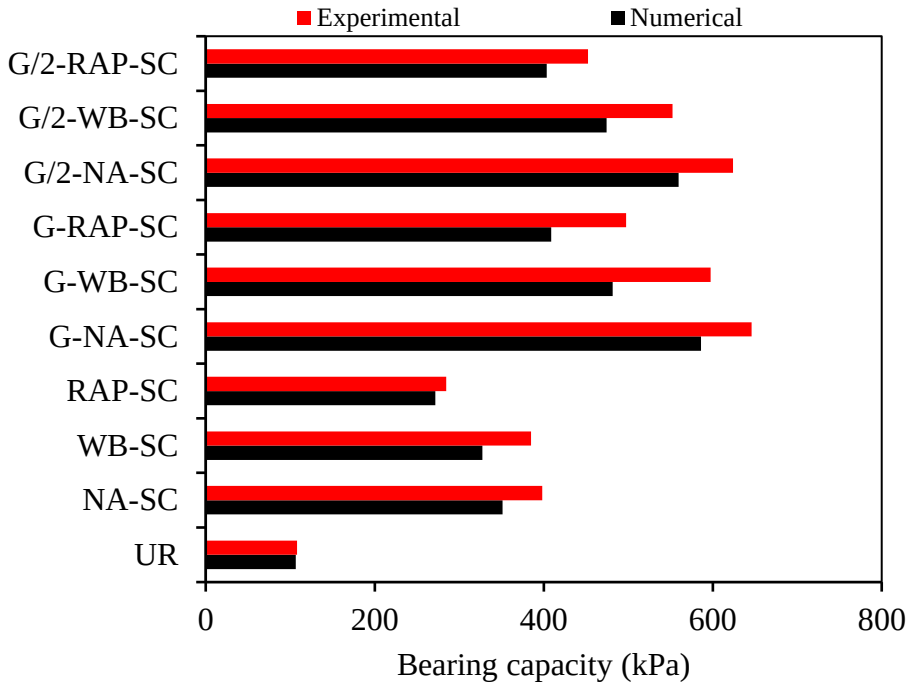

Figure 4.11. Numerical and experimental results of the bearing capacity for the all series

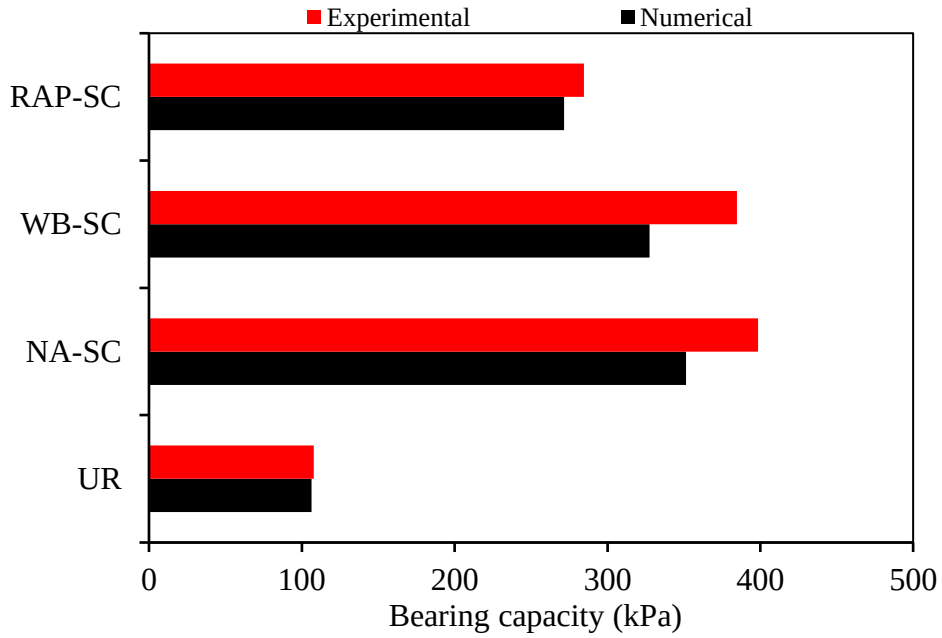

Figure 4.12. Numerical and experimental results of the bearing capacity for the series without geogrid encasement

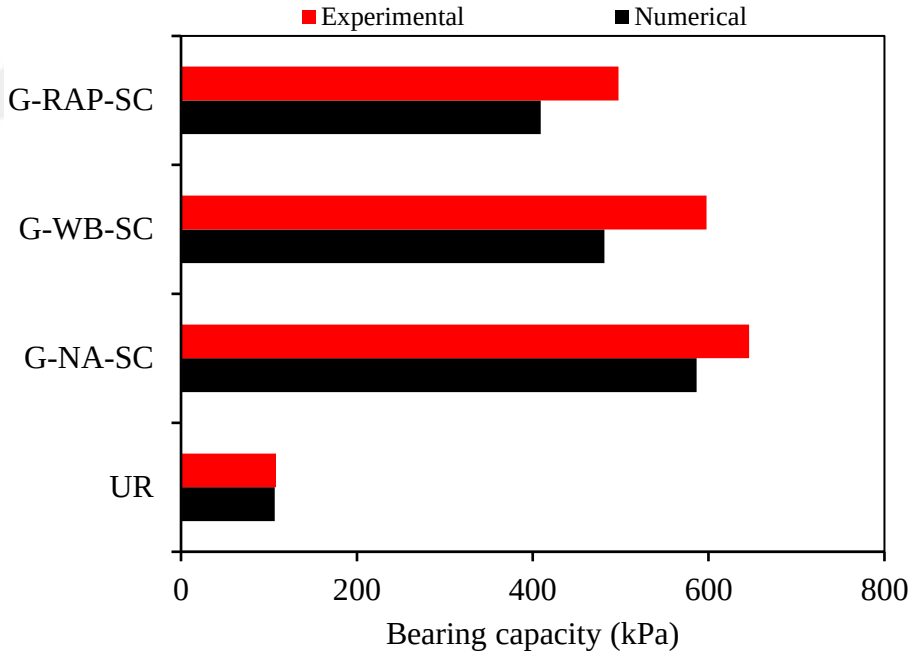

Figure 4.13. Numerical and experimental results of the bearing capacity for the series with 25 cm geogrid encasement

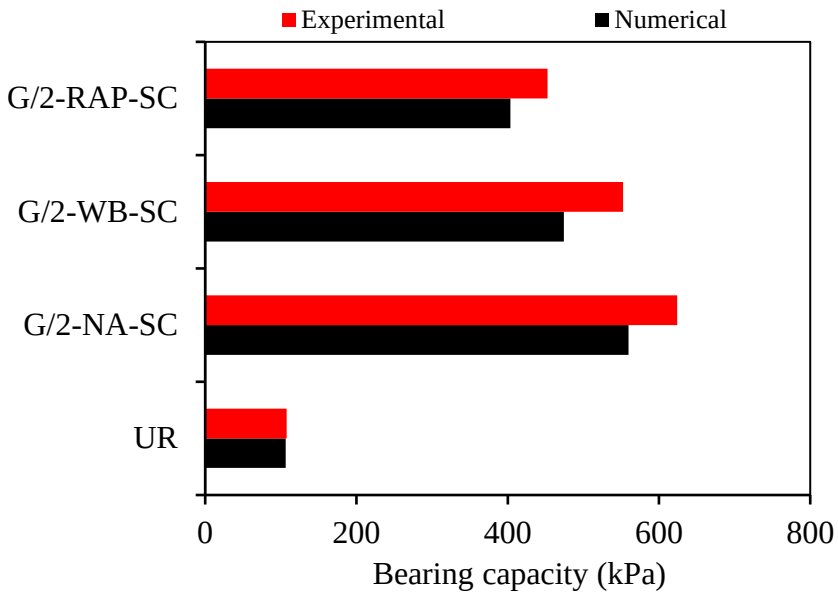

Figure 4.14. Numerical and experimental results of the bearing capacity for the series with 12.5 cm geogrid encasement

Table 4.1. Comparison of the numerical and experimental results

Samples	Numerical results (kPa)	Experimental results (kPa)
UR	106,42	107,92
NA-SC	351,44	398,44
WB-SC	327,53	384,82
RAP-SC	271,58	284,52
G-NA-SC	586,29	645,95
G-WB-SC	481,61	597,51
G-RAP-SC	408,93	497,63
G/2-NA-SC	559,71	624,08
G/2-WB-SC	474,31	552,57
G/2-RAP-SC	403,43	452,57

According to the results obtained from the reinforcement of the silty soil with geogrid-encasement decreased the settlement and increased the bearing capacity.

When the experimental results were compared within the scope of Kurt's thesis (2011), it was observed that the use of natural crushed stone in stone columns increased the bearing capacity.

Arulrajah et al. (2014) preferred recycled crushed brick, recycled asphalt pavement (RAP) and recycled concrete aggregate. They determined that these materials

have the potential for the use in road-base and sub-base applications because they possess the necessary minimum effective friction angles. Therefore, the materials used within the scope of this thesis can be preferred in the road-base and sub-base applications as they have a specific strength capacity.

Mohammadinia et al. (2014) preferred recycled crushed brick, recycled asphalt pavement (RAP) and recycled concrete aggregate. They indicated that cement-stabilized construction and demolition waste materials were suitable construction materials for road-base and sub-base applications.

Cabalar et al. (2016) examined that the use of construction and demolition waste materials in the soil resulted in an increase in the CBR value in their study. Within the context of their study, it was observed to increase the CBR value of the soil. Within the scope of both studies, the use of recycled materials provided environmental benefits.

According to the result of experimental studies conducted by Demir & Sarici (2016), the geogrid-encased stone column method improved the bearing capacity of the soil. In both experimental studies, the lateral bulging was generally observed to be more on the top of the stone column.

According to results of the experimental studies conducted by Demir & Sarici (2017), the reinforcement of the soil with stone column method and geogrid-encased stone column was examined to decrease the settlement and increase the bearing capacity.

The numerical analysis was conducted for undrained and sudden loading conditions similar to the experimental studies. Mohr Coulomb (MC) model was selected to model the behaviour of silt soil, natural crushed stone, rap, and waste brick. It was observed that the soil behavior can be effectively modeled by using the numerical analyses conducted in this way. The numerical analyses yielded results that closely matched the outcomes of the experimental studies.

The experimental studies produced graphs that exhibited fluctuations in certain areas, which could be due to the sudden failure or collapse of natural crushed stone, waste brick, and recycled asphalt pavement materials, or their abrupt penetration into the silty soil. On the other hand, the graphs obtained from numerical analyses were smoother.

It is evident that there is a growing potential for the use of stone column soil improvement method and geogrid-encased stone columns. The use of materials like geogrid can help to laterally confine and strengthen the stone column, and numerical analysis provides a practical method for studying the behavior of stone columns.

5. CONCLUSIONS

The thesis aimed to estimate the bearing capacity of a silty soil that is mixed crushed natural stones, recycled asphalt pavement, waste bricks and encased by geogrid using the stone column method. Ten series of tests were conducted in the laboratory for the experimental study. Also, it aimed to compare and validate the experimental results by PLAXIS for the unreinforced silty soil with those of reinforced with construction demolition wastes and geogrid encasement.

5.1. Conclusions of the Experimental Study

For all experiments, the silty soil model foundation had a fixed diameter of 5 cm and a height of 25 cm. Results from the experiments were calculated based on 10% of the foundation diameter. The experimental findings were as follows:

a) The study showed that using the stone column method to reinforce silty soil with natural crushed stone material increased bearing capacity by 3.69 times. Similarly, reinforcing silty soil with waste brick material increased bearing capacity by 3.57 times, and reinforcing silty soil with recycled asphalt pavement material increased bearing capacity by 2.64 times.

b) According to the study, reinforcing silty soil with natural crushed stone and a geogrid encasement of 25 cm height increased bearing capacity by 5.99 times. Similarly, using a geogrid encasement of 12.5 cm height increased bearing capacity by 5.78 times.

c) The study investigated reinforcing silty soil with waste brick and a geogrid encasement of 25 cm height, which increased bearing capacity by 5.54 times. Similarly, using a geogrid encasement of 12.5 cm height increased bearing capacity by 5.12 times.

d) Reinforcing silty soil with recycled asphalt pavement and a geogrid encasement of 25 cm height was observed to increase bearing capacity by 4.61 times. Similarly, using a geogrid encasement of 12.5 cm height increased bearing capacity by 4.19 times for the same mixture.

e) According to the experimental study, it has been determined that there was not much difference in terms of the effect on bearing capacity between using geogrid with a height of 25 cm and using geogrid with a height of 12.5 cm for stone column construction. Besides, lateral bulging was determined to be more in the upper parts of the stone column.

f) Reinforcing silty soil with natural crushed stone resulted in the highest increase in bearing capacity, followed by waste bricks and recycled asphalt pavement.
g) Based on the findings, reinforcing silty soil with construction demolition materials and geogrid encasement reduced settlement and increased bearing capacity.

5.2. Conclusions of the Numerical Analyses

The researchers utilized PLAXIS, a software based on finite element analysis, to conduct a numerical analysis that incorporated all the experimental conditions from the geotechnical laboratory. The bearing capacity values obtained from the numerical analysis were based on settlement values equivalent to 10% of the foundation diameter. Based on this, the following outcomes were established.

a) Reinforcing silty soil with natural crushed stone material increased the bearing capacity by 3.30 times, while using waste brick material increased the bearing capacity by 3.07 times. Similarly, reinforcing silty soil with recycled asphalt pavement material increased the bearing capacity by 2.55 times.
b) The study found that adding natural crushed stone to silty soil, reinforced with geogrid encasement of 25 cm height, increased the bearing capacity by 5.50 times. Similarly, using geogrid encasement of 12.5 cm height increased the bearing capacity by 5.26 times.
c) According to the study, using waste brick to reinforce silty soil with a geogrid encasement of 25 cm height increased the bearing capacity by 4.53 times. A similar mixture of stone column with geogrid encasement of 12.5 cm was found to increase the bearing capacity by 4.46 times.
d) The study showed that reinforcing silty soil with recycled asphalt pavement and a geogrid encasement of 25 cm height increased the bearing capacity by 3.84 times while using a geogrid encasement of 12.5 cm height increased the bearing capacity by 3.79 times.
e) According to the numerical study, it was found that there was not a significant difference in the impact on bearing capacity between using geogrid with a height of 25 cm and using geogrid with a height of 12.5 cm for stone column construction.
f) The findings from both numerical analyses and experimental studies were consistent with each other. The numerical analyses yielded results that closely matched the outcomes of the experimental studies.

g) The experimental data displayed considerable fluctuations on the graphs, which was attributed to the abrupt failure or collapse of the natural crushed stone, waste brick, and recycled asphalt pavement materials, or their sudden introduction into the silty soil matrix. Conversely, the numerical analyses exhibited a more consistent pattern.

REFERENCES

Adeli, N. (2013). *Taş kolonların analiz ve tasarımı*. [Master thesis, Çukurova University]. Yüksek Öğretim Kurulu Ulusal Tez Merkezi.

Ambily, A. P., & Gandhi, S. R. (2007). Behavior of stone columns based on experimental and FEM analysis. *Journal of geotechnical and geoenvironmental engineering*, 133(4), 405-415.

Arulrajah, A., Piratheepan, J., Bo, M. W., and Sivakugan, N. (2012). Geotechnical characteristics of recycled crushed brick blends for pavement sub-base applications, *Canadian Geotechnical Journal*, **49**, 7, 796-811.

ASTM C127-12, (2012). Standard Test Method for Density, Relative Density (Specific Gravity), and Absorption of Coarse Aggregate, ASTM International, West Conshohocken, PA

ASTM C127-12, (2012). Standard Test Method for Density, Relative Density (Specific Gravity), and Absorption of Coarse Aggregate, ASTM International, West Conshohocken, PA

ASTM C131-06, (2006). Standard Test Method for Resistance to Degradation of Small-Size Coarse Aggregate by Abrasion and Impact in the Los Angeles Machine, ASTM International, West Conshohocken, PA.

ASTM C136-06, (2006). Standard Test Method for Sieve Analysis of Fine and Coarse Aggregates, ASTM International, West Conshohocken, PA.

ASTM D1140- 00 (2006). standard test methods for amount of material in soils finer than No. 200 (75-μm) Sieve. ASTM International, West Conshohocken, PA.

ASTM D2166-06. (2006) Standard test method of unconfined compressive strength of cohesive soil. ASTM International, West Conshohocken, PA.

ASTM D2487- 11 (2011). Standard practice for classification of soils for engineering purposes (Unified Soil Classification System). ASTM International, West Conshohocken, PA.

ASTM D422- 63 (2007). Standard test method for particle-size analysis of soils. ASTM International, West Conshohocken, PA.

ASTM D854-02 (2002). Standard test methods for specific gravity of soil solids by water Pycnometer. ASTM International, West Conshohocken, PA.

ASTM D854-10, (2010). Standard Test Methods for Specific Gravity of Soil Solids by Water Pycnometer, ASTM International, West Conshohocken, PA.

Das, P., & Pal, S. K. (2013). A study of the behavior of stone column in local soft and loose layered soil. *EJGE*, 18, 1777-17786.

Deb, K., Samadhiya, N. K., & Namdeo, J. B. (2011). Laboratory model studies on unreinforced and geogrid-reinforced sand bed over stone column-improved soft clay. *Geotextiles and Geomembranes*, 29(2), 190-196.

Debnath, P., & Dey, A. K. (2017). Bearing capacity of geogrid reinforced sand over encased stone columns in soft clay. *Geotextiles and Geomembranes*, *45*(6), 653-664.

Debnath, P., & Dey, A. K. (2018). Prediction of bearing capacity of geogrid-reinforced stone columns using support vector regression. *International Journal of Geomechanics*, *18*(2), 04017147.

Demir, A., & Sarici, T. (2016). Bearing capacity and bulging behavior of Geogrid encased stone columns. *Selcuk University Journal of Engineering, Science & Technology/Selçuk Üniversitesi Mühendislik, Bilim ve Teknoloji Dergisi*, 4(2), 131-144.

Demir, A., & Sarici, T. (2017). Bearing capacity of footing supported by geogrid encased stone columns on soft soil. *Geomech. Eng*, 12(3), 417-439.

Demir, A., Sarici, T., Laman, M., Bagriacik, B., & Ok, B. (2013). An experimental study on behaviour of geosynthetic reinforced stone columns. In *2nd International Balkans Conference on Challenges of Civil Engineering*. 23-25 May 2013, 832-841.

Elsawy, M., Lesny, K., & Richwien, W. (2010). Performance of geogrid-encased stone columns as a reinforcement of soft ground. In *Numerical Methods in Geotechnical Engineering* (pp. 891-896). CRC Press.

Fahmi, K. S., & Kolosov, E. (2018). Behaviour of the clay soil reinforced by stone column encased with geogrid under cyclic load. *Ekologiya i Stroitelstvo*, 1, 33-38.

Fattah, M. Y., & Majeed, Q. G. (2012). Finite element analysis of Geogrid encased stone columns. *Geotechnical and Geological Engineering*, *30*, 713-726.

Ghanizadeh, A. R., Ghanizadeh, A., Asteris, P. G., Fakharian, P., & Armaghani, D. J. (2023). Developing bearing capacity model for geogrid-reinforced stone columns improved soft clay utilizing MARS-EBS hybrid method. *Transportation Geotechnics*, *38*, 100906.

Gniel, J., & Bouazza, A. (2009). Improvement of soft soils using geogrid encased stone columns. *Geotextiles and Geomembranes*, *27*(3), 167-175.

Gniel, J., & Bouazza, A. (2010). Construction of geogrid encased stone columns: A new proposal based on laboratory testing. *Geotextiles and Geomembranes*, *28*(1), 108-118.

Gu, M., Zhao, M., Zhang, L., & Han, J. (2016). Effects of geogrid encasement on lateral and vertical deformations of stone columns in model tests. *Geosynthetics International*, *23*(2), 100-112.

Gu, M., Han, J., & Zhao, M. (2017). Three-dimensional discrete-element method analysis of stresses and deformations of a single geogrid-encased stone column. *International Journal of Geomechanics*, *17*(9), 04017070.

Gu, M., Han, J., & Zhao, M. (2020). Three-dimensional DEM analysis of axially loaded geogrid-encased stone column in clay bed. *International Journal of Geomechanics*, *20*(3), 04019180.

Gu, M., Mo, H., Qiu, J., Yuan, J., & Xia, Q. (2022). Behavior of floating stone columns reinforced with geogrid encasement in model tests. *Frontiers in Materials*, *9*, 980851.

Jianfeng, C. H. E. N., Sen, M. E. I., & Shouzhong, F. E. N. G. (2019). Uniaxial compression tests of biaxial geogrid-encased stone columns. *工程地质学报*, *27*(2), 311-316.

Kim, J., Son, S., Mahmood, K., & Ryu, J. (2012). Site response and shear behavior of stone column-improved ground under seismic loading. In *Proceeding of the 15th worlds conference on earthquake engineering*. January 2017, 1-8.

Kurt, E. (2011). *Darbeli kırmataş kolon ve taş kolon elemanlarına ait yükleme testlerinin sayısal analizi ve sonuçlarının karşılaştırılması* [Master thesis, İstanbul Technical University]. Yüksek Öğretim Kurulu Ulusal Tez Merkezi.

Kwa, S. F., Kolosov, E. S., & Fattah, M. Y. (2018). Ground improvement using stone column construction encased with geogrid. *Stroitel'stvo Unikal'nyh Zdanij i Sooruzenij*, (3), 49-59.

Malarvizhi, S. N., & Ilamparuthi, K. (2007). Comparative study on the behavior of encased stone column and conventional stone column. Soils and foundations, 47(5), 873-885.

Marto, A., Moradi, R., Helmi, F., Latifi, N., & Oghabi, M. (2013). Performance analysis of reinforced stone columns using finite element method. *Electronic Journal of Geotechnical Engineering*, 18, 315-323.

Modarres, A., and Nosoudy, Y. M. (2015). Clay stabilization using coal waste and lime-technical and environmental impacts, *Applied Clay Science*, **116**, 281-288.

Nazari Afshar, J., & Ghazavi, M. (2014). Experimental studies on bearing capacity of geosynthetic reinforced stone columns. *Arabian Journal for Science and Engineering*, 39, 1559-1571.

Pandey, B. K., Rajesh, S., & Chandra, S. (2020, February). Numerical evaluation of geogrid-encased stone columns in soft soil under embankment loading. In *Geo-*

Congress 2020: Foundations, Soil Improvement, and Erosion (pp. 543-551). Reston, VA: American Society of Civil Engineers

Paul, A., & Ponomarjow, A. (2004). The bearing behavior of geogrid reinforced, crushed stone columns in comparison to non-reinforced concrete pile foundations. *Proceedings of the Eurogeo, 3*, 285-289.

Rajesh, S. (2017). Time-dependent behaviour of fully and partially penetrated geosynthetic encased stone columns. *Geosynthetics International*, 24(1), 60-71.

Rathod, D., Abid, M. S., & Vanapalli, S. K. (2021). Performance of polypropylene textile encased stone columns. *Geotextiles and Geomembranes*, 49(1), 222-242.

Reddy, C. S., & Mohanty, S. (2017). Seismic behavior of stone column on a sloping layered soil. In *6th Indian Young Geotechnical Engineers Conference, 6IYGEC-2017, March 2017*, 1-4.

Safiuddin, M., Jumaat, M. Z., Salam, M. A., Islam, M. S., & Hashim, R. (2010). Utilization of solid wastes in construction materials. *International journal of physical sciences*, 5(13), 1952-1963.

Sarıcı, T. (2014). *Geosentetik ile güçlendirilmiş taş kolonların taşıma kapasitesinin analizi*. [Master thesis, İnönü University]. Yüksek Öğretim Kurulu Ulusal Tez Merkezi.

Sarıcı, T. Demir, A. Altay, G. Laman, M. Ok, B. Bağrıaçık, B. (2013). Experimental evaluation of stone column in soft clay with small scale tests. 5. Geoteknik Sempozyumu.

Tan, X., Hu, Z., Chen, C., & Zhao, M. (2021). 3D DEM-FDM coupled analysis of the behavior of an isolated geogrid-encased stone column under axial loading. *Journal of Geotechnical and Geoenvironmental Engineering*, *147*(6), 04021028.

Xu, F., Moayedi, H., Foong, L. K., Moghadam, M. J., & Zangeneh, M. (2021). Laboratory and numerical analysis of geogrid encased stone columns. *Measurement*, *169*, 108369.

Yashwant, A.K., Owais, S.M. and Dasaka, S.M. (2011). Behaviour of stone column reinforced marine clay under static and cyclic loading. *Proceding of Indian Geotecnical Conference*, Kochi, (Paper No: H-133), 15-17 December 2011, 429-432.

Yoo, C., & Abbas, Q. (2020). Laboratory investigation of the behavior of a geosynthetic encased stone column in sand under cyclic loading. *Geotextiles and Geomembranes*, 48(4), 431-442.

Zahmatkesh, A., & Choobbasti, A. J. (2010). Settlement evaluation of soft clay reinforced by stone columns, considering the effect of soil compaction. *International Journal of Research and Reviews in Applied Sciences*, 3(2), 159-166.